國立交通大學

物理研究所

碩士論文

氫原子在不同偏振光的 Pump 和 Probe 雷射照射下之效應

Polarization Effect of Pump-Probe Process on Hydrogen Atom

研 究 生：吳明軒

指導教授：江進福　教授

中華民國九十九年七月

氫原子在不同偏振光的Pump和Probe雷射照射下之效應
Polarization Effect of Pump-Probe Process on Hydrogen Atom

研 究 生：吳明軒　　Student：Ming-Hsuan Wu

指導教授：江進福　　Advisor：Tsin-Fu Jiang

國立交通大學

物理研究所

碩士論文

A Thesis Submitted to Institute of Physics College of Science
National Chiao Tung University in partial Fulfillment of the
Requirements for the Degree of Master in

Physics

June 2010

Hsinchu, Taiwan, Republic of China

中華民國九十九年七月

氫原子在不同偏振光的 Pump 和 Probe 雷射照射下之效應

學生：吳明軒　　指導教授：江進福

國立交通大學物理研究所碩士班

摘要

氫原子在雷射 pump 和 probe 照射下，利用由 N. N. Choi 和 T. F. Jiang 等人所建立的 pump-probe 模型，計算當氫原子在 pump 雷射照射後，接著照射一 probe 雷射來獲取干涉過程之資訊。並改變 probe 雷射之方向，計算其不同偏振下的效應。

Polarization Effect of Pump-Probe Process on Hydrogen Atom

Student：Ming-Hsuan Wu Advisor：Dr. Tsin-Fu Jiang

Institute of Physics

National Chiao Tung University

ABSTRACT

In pump-probe process, the probe laser was applied to retrieve the information of electron's dynamics on atoms or molecules after the pump laser process finished. In this thesis, we used the pump-probe model constructed by N. N. Choi and T. F. Jiang et al., to investigate the interference effect on the hydrogen atom. Besides, we used linear and elliptical polarization on probe laser to study how polarization effect affected on the hydrogen atom in pump-probe process.

誌謝

感謝指導教授江老師耐心得指導，每次的 meenting、課程上以及討論都讓我獲益良多，激發很多在論文上的想法以及學習研究的方法，也讓我明瞭理論模型在物理學上的重要性。也非常感謝博士後研究員的李漢傑博士和鄭世達學長，在我對理論知識不足的情況下，總是犧牲自己的研究時間耐心地教導我、替我尋找有用的資料，補足我對論文題目的了解。在我對 LINUX 作業系統以撰寫程式上有迷惑時，感謝李允民博士和鄭玉書同學的幫忙和協助。也感謝曾給予建議協助的師長們，以及在夜晚寂靜地研究室陪伴我敲打電腦的學長張繼允和奈米所學弟謝孟哲，還有在剛踏入交大校園裡帶我認識物理所的徐煥鈞學長，感謝。

在研究的過程中，支持著每一步往前進的動力，除了對物理感到好奇的這份拉力，家人總是在身後默默給予支持。感謝老媽、老樺、大哥和女友的照顧、支持、電話的問候和寫作論文上的幫助，你們是我前進的主要動力，也是我這一生最重要的人，我愛你們。

要感謝的人還很多，在新竹的大學同學，以前大學教授和大學室友等等，但唯一最好的回報，就是不會辜負你們對我的期望，繼續努力。

目錄

符號說明

$|M_{if}|^2$ ：The angle-resolved photoelectron probability density

t_d ：The time delay

ε_k ：Photoelectron energy

θ_k, φ_k ：The polar and azimuth angle of photoelectron emissive direction

θ_l, φ_l ：The polar and azimuth angle of Probe laser pulse's direction under dipole approximation

P ：The total probability of photoelectron ionization

$\frac{dP}{d\varepsilon_k}$ ：The energy-resolved photoelectron probability density

α ：The ratio of x and z direction amplitude of probe electric field

List of Figure

Chapter 1

Introduction

In recent years, the attosecond science is very popular to measure the electron dynamics on its nature time scale, the time of that an electron make a cycle on atom, which is about 24 attoseconds. In pump-probe experiements, try to apply a pump laser with time delay between the probe laser which interfering on the wave packets with the pump laser and has the goal to unravel the dynamics of atoms or molecules. Such experiments have the advantage that the time delay can be controlled with high precision at the level of attoseconds. There are two type of attosecond pulse can be produced in the laboratory. One is the single attosecond pulse (SAP), wider spread in frequency for short pulse duration, and the other one is attosecond pulse trains (APT) , which in the extreme ultraviolet can be produced in the process of high-order harmonic generation (HHG) by exposing rare gas atoms to intense femtosecond infrared (IR) laser pulses. To see the difference between SAP and APT in time and energy domain in Fig. 1.1. The width spread in frequency can be calculated by $\Delta\omega = 4\ln 2/\Delta\tau$, where the $\Delta\omega$ is the pulse's full width of half maximum (FWHM) in frequency domain and the $\Delta\tau$ stands for the pulse duration of FWHM, so the $\Delta\omega \approx 1.83/\Delta\tau$, $\Delta\tau$ in fs unit. Thus today only a handful of laboratories are capable of performing APT+IR or SAP+IR experiments, where the IR is the femtosecond infrared (IR) laser pulses. N. N. Choi and the T. F. Jiang, etc. construct a simple theory[1], a pump-probe model , analytically and successfully to explane the pump-probe experiments. Here , we use the APT+IR process as they do.

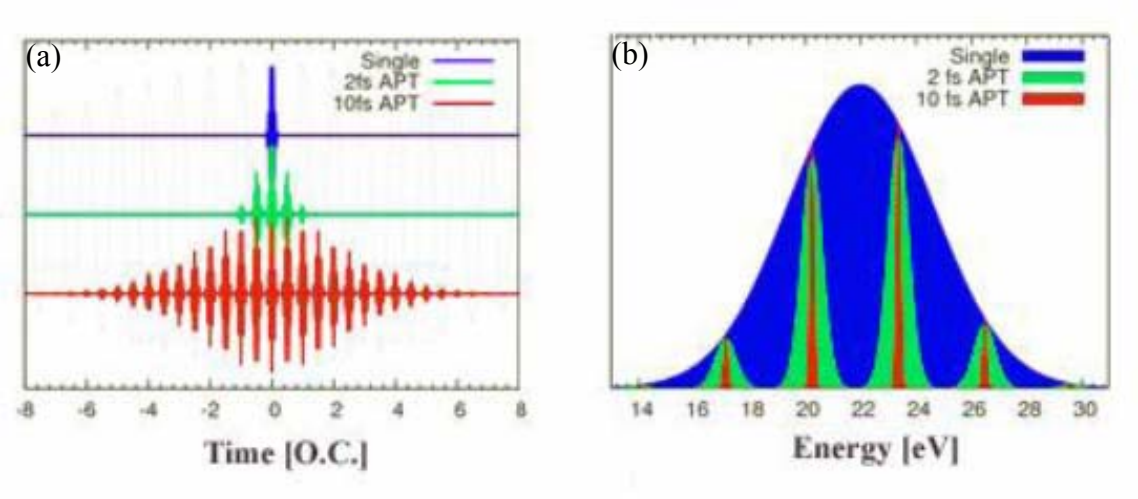

Figure. 1.1 The SAP and APT in (a) time domain and (b) energy domain. The width of FWHM for blue, green and red pulse is 6ev, 0.9ev, and 0.183 ev. (P. Ranitovic et al., 2010[2])

The APT are synthesized from the high harmonics generated by HHG in plateau region, as showed in Fig. 1.2

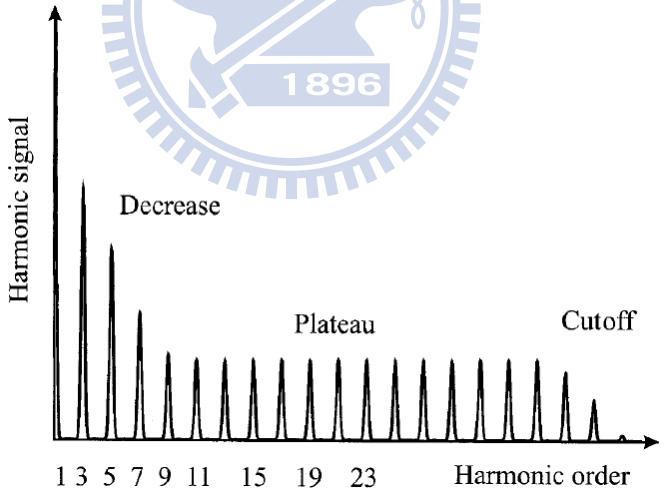

Figure. (1.2) The typical high-harmonics spectrum

The form of APT pulse can be written down as

$$E(t) = E_0 \sum_{n=11}^{n=29} \sin(n\omega t + \varphi), n = odd \qquad (1.1)$$

where the E_0 is the APT pulse envelope, and the the carrier envelope phase (CEP) φ is fixed.

In this thesis, we simulate the APT pulse on the hydrogen atom to dissus the pump-probe process, and then briefly introduce the pump-probe model by the T. F. Jiang, etc. in chapter 2. In chapter 3, we introduce only considering one excited state system, Ψ_{210} on hydrogen atom, and show the numerical result. Futermore, In chapter 4 consider two excited states, Ψ_{310} and Ψ_{410}, in the pump-probe model which totally three wave packets interfere with each other, and then show the numerical result. In chapter 5, consider the linear polarization effect by aligning the probe laser to different direction between pump laser to retrieve the information in pump-probe process. Finall, the last chapter, chapter 6, is the conclusions about this thesis.

chapter 2.

Pump-probe model

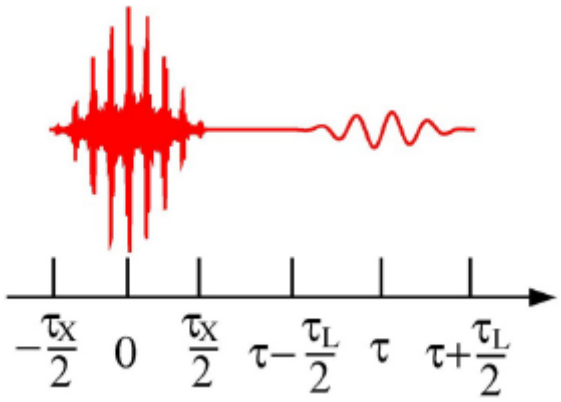

Figure. (2.1) The diagram for pump APT pulse and probe IR pulse in time domain in pump-probe process.

In pump probe model, there are two pulse laser, pump and probe laser, applied to the target, and here we use hydrogen as the target. The first laser coming into the system called first path for the interference uses APT (Attosecond Pulse Trains) pulse as pump laser, and then the second laser called second path for the interference uses IR pulse to be the probe laser. APT pulse can drive the electron of the hydrogen to jump probably to continuum state and excited state, if the APT pulse's for some high-harmonics frequency (to see Eqs. (1.1))are nearly resonant for some excited states. Then, a time delay after the APT pulse ending, the IR pulse comes into the system and has weaker energy then APT pulse to contribute the probability for the electron from the excited state to the continuum state. Finally, the two paths will interfere with each other in the energy spectrum.

In the beginning of pump-probe process, define t=0 to be at the center of the APT pulse. The time difference between the APT pulse's center and IR pulse's center is defined as the time delay τ. For clarity, the Hamiltonian of such a dynamic system can be written in the

dipole approximation as

$$H = H_0 + zE_x(t) + \vec{\varepsilon}\cdot\hat{r}E_L(t-\tau) \tag{2.1}$$

where, the APT pulse is aligned to parallel with z axis, and for being interested in the effect about the different laser direction between APT pulse and the IR pulse, we applied the IR pulse direction at $\vec{\varepsilon}\cdot\hat{r}$.

To consider only the situation in that the pump and probe laser do not overlap, so we can write down the total evolution operator (propagator) for the pump and probe laser as

$$U_{total} = U_L(\tau + \tau_L/2, \tau - \tau_L/2)\cdot e^{-iH_0 t_d}\cdot U_x(\tau_x/2, -\tau_x/2) \tag{2.2}$$

where, the t_d is defined to the time different between the APT pulse ending and the IR pulse starting, and the $e^{-iH_0 t_d}$ is the propagator of Hamiltonian under no any external field. Represent the atomic evolution operator $e^{-iH_0 t_d}$ in terms of the excited (bounded state) and continuum eigenstate , |n>, and eigenenergy E_n of H_0

$$e^{-iH_0 t_d} = \sum_n |n> e^{-iE_n t_d} <n| \tag{2.3}$$

Therefore, the total evolution operator U_{total} can be rewriten to

$$U_{total} = \sum_n U_L(\tau + \tau_L/2, \tau - \tau_L/2)\cdot |n> e^{-iE_n t_d} <n|\cdot U_x(\tau_x/2, -\tau_x/2) \tag{2.4}$$

Write down the transition probability amplitude as a function of time-delay for transit from initial bound state $|i>$ to an final ionized state $|f>$

$$\begin{aligned} M_{i\to f} &= <f|U_{total}|i> = M_{if} \\ &= \sum_n <f|U_L(\tau + \tau_L/2, \tau - \tau_L/2)|n>\cdot e^{-iE_n t_d}\cdot <n|U_x(\tau_x/2, -\tau_x/2)|i> \end{aligned} \tag{2.5}$$

From Eqs. (2.5), the ionization process under the pump-probe pulse as a coherent sum of

paths represented by the intermediate state $|n>$, and the transition amplitude is contributed from the intermediate state $|n>$ to the final ionized state $|f>$. The APT pulse can pump the electron probably to some excited states of hydrogen atom and ionized state, so we choose the intermediate state as bounded state and unbounded state. In chapter 3, we consider continuum state and only one bounded state to be intermediate states. In chapter 4, we add one more bounded state, two bounded states, and continuum state to be intermediate states.

Chapter 3.

Considering one excited state in pump-probe model

For considering one excited state in pump-probe model, we choose first excited state of hydrogen atom $|2p>$ as bounded state, and another one is continuum state $|k'>$ as unbounded state. The electron in ground state is ionized by the first laser, APT pulse that we simulating only two high-harmonic orders frequency, one makes the probability to excite to the unbounded state, the second one to ionize to continuum state $|k'>$, and finally is driven to the other continuum state $|k>$ by the second laser, IR pulse. There are two paths interfering with each other at same energy spectrum. To describe the dynamics system, as showed in Fig. 3.1.

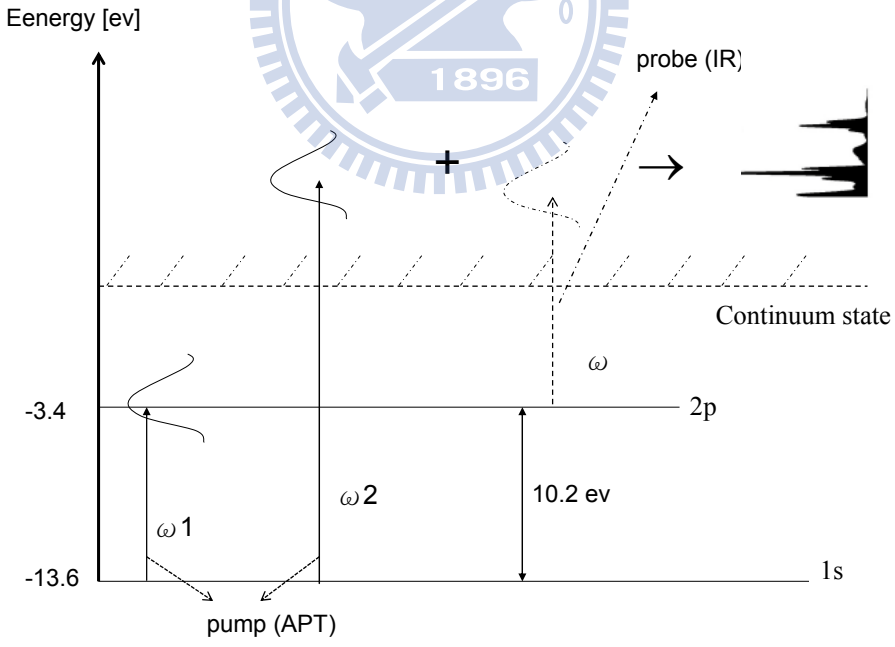

Figure. 3.1 The mechanics for considering one excited state in pump-probe model. The ω1 = 10.1 ev, ω2 = 15.1 ev, ω= 5 ev

In the Fig. 3.1, the beginning of the electron in initial ground state $|1s>$ is probably ionized by the APT pulse to the first excited state $|2p>$ and continuum state $|k'>$, and then driven to the continuum state $|k>$ by the IR pulse in weak frequency to the same energy spectrum. We let the initial, intermediate and final state as

$$\begin{aligned} |i>&=|1s> \\ |f>&=|k> \\ |n>&=|2p> \; and \; |k'> \end{aligned} \tag{3.1}$$

here (and throughout the thesis) $|k>$ dose not denote a plane wave but a scattering wave which is an eigenstate of H_0 with incoming boundary conditions. Therefore, for considering one excited state in pump-probe model, we can write down the transition probability amplitude as

$$M_{if} = e^{-iE_{2p}t_d} M_{k,2p} M_{2p,1s} + \sum_{k'} e^{-i\varepsilon_{k'}t_d} M_{k,k'} M_{k',1s} \tag{3.2}$$

where the $M_{2p,1s}$, and $M_{k',1s}$ are probability amplitudes for transition induced by the APT pulse, and the $M_{k,2p}$ and $M_{k,k'}$ are the probability amplitudes for transition induced by the probe IR laser pulse, and the E_{2p} and ε_k are the eigenenergy of H_0 for $|2p>$ state and the $|k'>$ state.

For the intermediate state $|k'>$ transition to the continuum state $|k>$, the free electron does not change the momentum and the energy by the IR laser pulse but accumulates the phase which is called Volkov phase during the free electron propagating time. To use the Volkov phase approximation

$$M_{k,k'} = \delta(k-k') \exp[-\frac{i}{2}\int_{-\frac{\tau_L}{2}}^{\frac{\tau_L}{2}} (\vec{k}+\vec{A}(t))^2 dt] \tag{3.3}$$

where $\vec{A}(t)$ is the vector potential of the probe IR laser pulse. Finally, the transition probability amplitude can be rewritten clearly as

$$M_{if} = e^{-iE_{2p}t_d} M_{k,2p} M_{2p,1s} + e^{-i\varepsilon_k t_d} e^{-i(\tau_L \cdot \varepsilon_k + \vec{\alpha}\cdot\vec{k} + \beta)} M_{k,1s} \tag{3.4}$$

where

$$\vec{\alpha} = \int_{\tau - \frac{\tau_L}{2}}^{\tau + \frac{\tau_L}{2}} \vec{A}(t-\tau)dt \quad \text{and} \quad \beta = \int_{\tau - \frac{\tau_L}{2}}^{\tau + \frac{\tau_L}{2}} A^2(t-\tau)dt \tag{3.5}$$

To change the variables, we can find the α and β are independent on the time delay τ.

$$\vec{\alpha} = \int_{-\frac{\tau_L}{2}}^{\frac{\tau_L}{2}} \vec{A}(t)dt \quad \text{and} \quad \beta = \int_{-\frac{\tau_L}{2}}^{\frac{\tau_L}{2}} A^2(t)dt \tag{3.6}$$

For clarity to see the magnitude and phase in the transition probability amplitude, we define that

$$\begin{aligned} M_{k,2p} &= < k \mid U_L \mid 2p > = b_{k,p} \cdot \exp(i\phi_{k,p}) \\ M_{2p,1s} &= < 2p \mid U_x \mid 1s > = a_{p,s} \cdot \exp(i\varphi_{p,s}) \\ M_{k,1s} &= < k \mid U_x \mid 1s > = a_{k,s} \cdot \exp(i\varphi_{k,s}) \end{aligned} \tag{3.7}$$

Finally, the ionization probability density is expressed as

$$\begin{aligned} &\mid M_{if}(t_d) \mid^2 = a^2{}_{k,s} + b^2{}_{k,p} a^2{}_{p,s} + a_{k,s} b_{k,p} a_{p,s} \cos\left[\ \Phi - (\varepsilon_k - E_{2p}) t_d\ \right] \\ &\Phi = \varphi_{k,s} - (\varepsilon_k \tau_L + \vec{\alpha}\cdot\vec{k} + \beta) - (\varphi_{p,s} + \phi_{k,p}) \end{aligned} \tag{3.8}$$

Eqs. (3.8) gives some information about the mechanism in pump-probe model. The first term gives the probability for producing an electron with momentum k by APT pulse. The second term is the probability for the electron exciting to the $\mid 2p >$ state by the APT, and then ionizing to the same continuum state $\mid k >$ with same final momentum k. The last term is due to the interference of the two different paths, where the time delay dependence is explicitly expressed clearly. The phase in cosinusoidal function including the phase of the excitation and ionization amplitude is contributed by the pump APT pulse and probe IR pulse, and dose not depend on the time delay t_d.

3.1 Two-level system

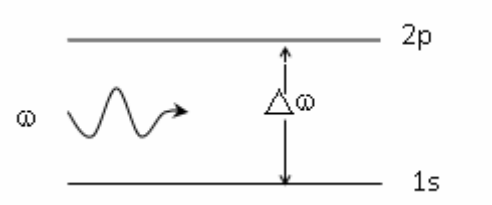

Figure 3.2. △ω=10.2 ev, ω=10.1 ev

Consider the interaction of a radiation electric field E(t) of energy ω with a two-level hydrogen atom system, $|1s>$ and $|2p>$ .Let $|1s>$ and $|2p>$ represent the hydrogen ground state (the lower level) , and excited state with quantum number n=2 and l=1 (the upper level). we can describe the total wave function in the form of

$$|\Psi(t)>= C_{1s}(t)|1s>+C_{2p}(t)|2p> \tag{3.9}$$

where $C_{1s}(t)$ and $C_{2p}(t)$ are the probability amplitudes of finding the electron in states $|1s>$ and. $|2p>$ In the interaction picture, we can let the time-dependent coefficient $C_{1s}(t) = c_{1s}(t)e^{-iw_a t}$, and the *Schrödinger* equation can chage to

$$|\Psi(t)>= c_{1s}(t)e^{-i\hbar\omega_{1s}t}(t)|1s>+c_{2p}(t)e^{-i\hbar\omega_{2p}t}|2p> \tag{3.10}$$

where $\hbar\,\omega_{1s}$ and $\hbar\,\omega_{2p}$ are the eigenenergy of $|1s>$ (≈ -13.6 ev) and $|2p>$ (≈ -10.2 ev).

The corresponding Hamiltonian of the *Schrödinger* equation is

$$H = H_0 + H' \tag{3.11}$$

where the unperturbed part Hamiltonian H_0 is

$$H_0 = \hbar\omega_{1s}|1s><1s|+\hbar\omega_{2p}|2p><2p| \tag{3.12}$$

and the perturbed part H' is

$$H' = E(t)\cdot\hat{z} = \hat{z}\cdot E_m \cdot \exp[-2\ln 2(t/\tau_X)^2]\cdot\cos(\omega t + \phi_X) \tag{3.13}$$

The unperturbed part H' Eqs. (3.13) ,where E_m is the maximum amplitude of electric field E(t), and τ_X is the duration time of E(t), and ϕ_X is the carrier envelope phase (CEP) of the pump APT pulse E(t).

The equation of motion for the amplitude coefficient $c_{1s}(t)$ and $c_{2p}(t)$ may be written as

$$\begin{aligned} i\dot{c}_{1s}(t) &= \frac{E_m}{2}\cdot e^{-i\Delta t} < 1s \mid z \mid 2p > c_{2p}(t) \\ i\dot{c}_{2p}(t) &= \frac{E_m}{2}\cdot e^{i\Delta t} < 2p \mid z \mid 1s > c_{1s}(t) \end{aligned} \tag{3.14}$$

In deriving the Eqs. (3.14), we have ignored the emission photon term, and only considered the absorbtion photon term propotional to $\exp[\pm i(\omega - (\Delta\omega)]$ on the right hand side in rotating wave approximation (RWA). Here, we use the 4th order Runge Kutta method (RK4) to solve the Eqs. (3.14).

Fianlly, we want to check my program, so use two special cases to check my program code. First, the case one is frequency of electric field equals resonant frequency ω. We derive the analytical solutions for the special calse when ω equals the resonance frequency $\Delta\omega$. Let the coefficient to

$$\begin{aligned} c_{1s} &= a_r + ia_i \\ c_{2p} &= b_r + ib_i \end{aligned} \tag{3.15}$$

and we can derive the analytical solutions as

$$
\begin{aligned}
a_r(t) &= \cos\{\Omega\sqrt{\frac{\pi}{a}}\frac{\tau}{2}[1 \mp erf(\frac{\sqrt{a}}{\tau}t)]\} \\
b_i(t) &= \sin\{\Omega\sqrt{\frac{\pi}{a}}\frac{\tau}{2}[1 \mp erf(\frac{\sqrt{a}}{\tau}t)]\} \\
t \le 0 &- >"+" \\
t \ge 0 &- >"-"
\end{aligned}
\tag{3.16}
$$

To use Eqs. (3.16) to compare my numerical result of RK4 method

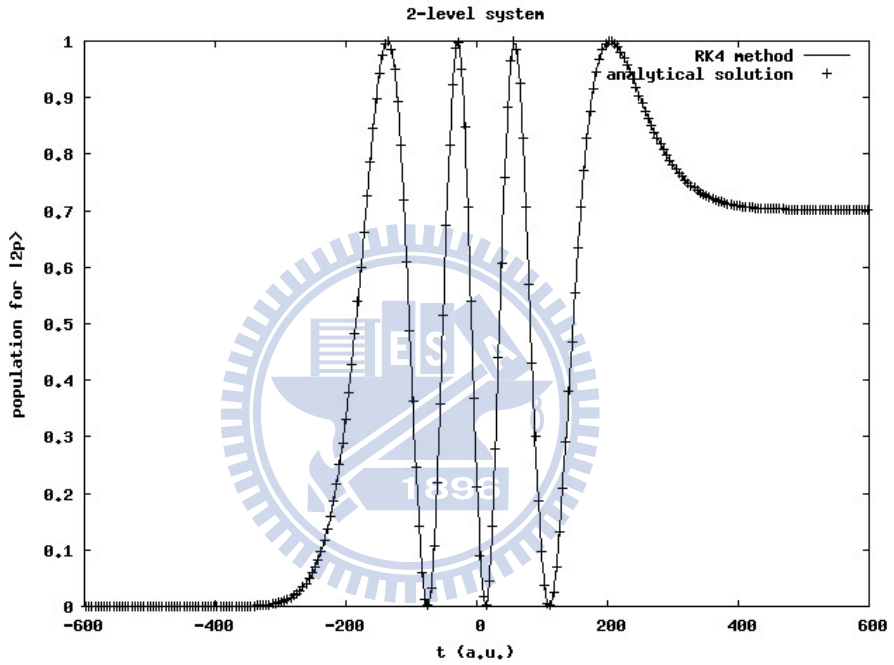

Figure. 3.3 The lines is by the RK4 method, and the points (+) are by the analytical solution. E_m=0.1 (a.u.), FWHM = 5 (fs). The result of RK4 well fits in with the analytical solution.

Secondly, the case two is for the electric field being no pulse's shape, like $E(t) = E_m \cos(\omega t)$ and the solution is (see [3])

$$
\Rightarrow \begin{cases}
C_{1s}(t) = \{\ C_{1s}(0)[\ \cos(\frac{\Omega t}{2}) - i\frac{\Delta}{\Omega}\sin(\frac{\Omega t}{2})\ ] + i\frac{\Omega_R}{\Omega}C_{2p}(0)\sin(\frac{\Omega t}{2})\ \}e^{i\Delta t/2} \\
C_{2p}(t) = \{\ C_{2p}(0)[\ \cos(\frac{\Omega t}{2}) + i\frac{\Delta}{\Omega}\sin(\frac{\Omega t}{2})\ ] + i\frac{\Omega_R}{\Omega}C_{1s}(0)\sin(\frac{\Omega t}{2})\ \}e^{-i\Delta t/2}
\end{cases}
\tag{3.17}
$$

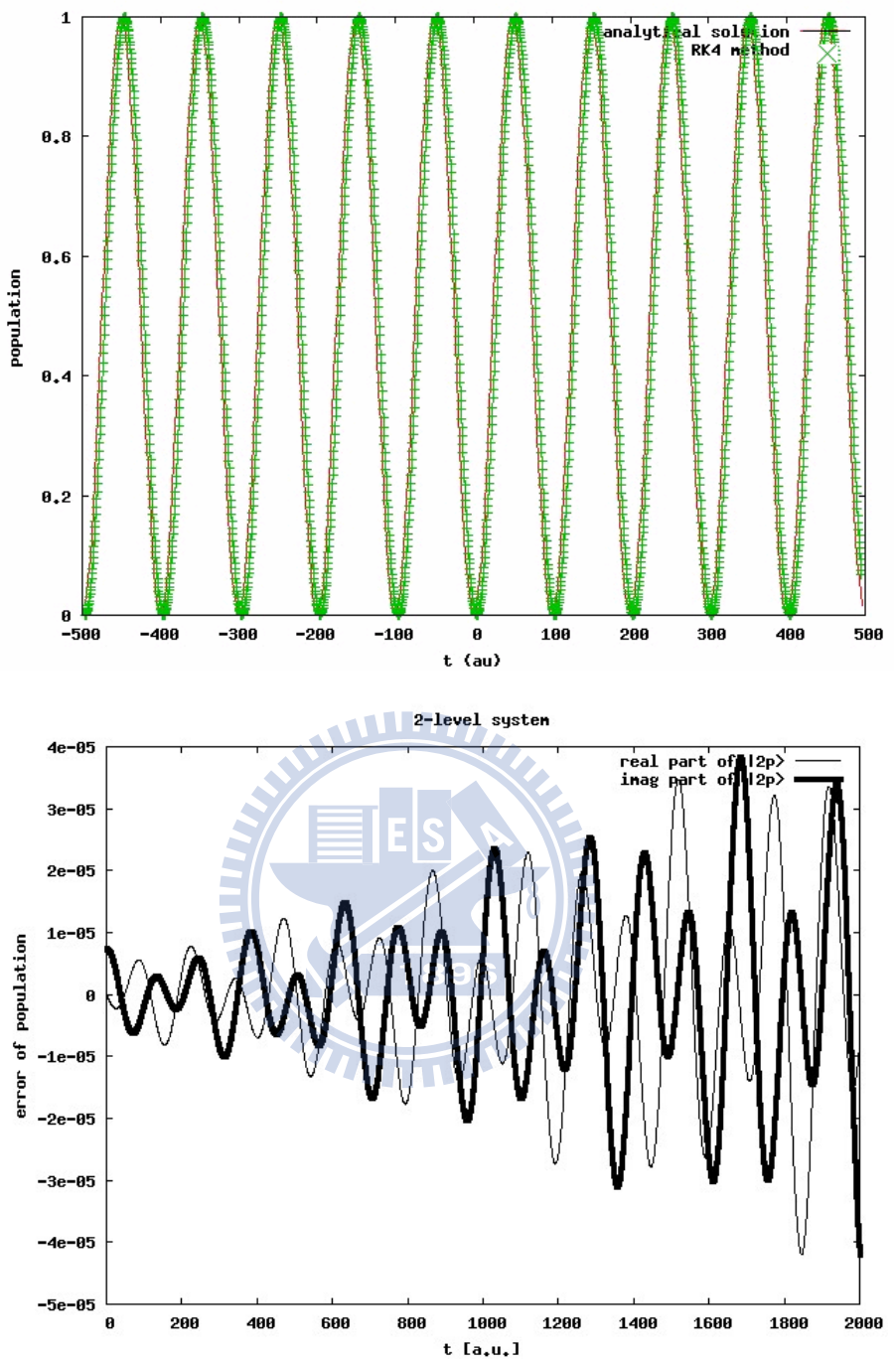

Figure. 3.4 E_m=0.1 (a.u.), $\Delta=\omega_{21}\times 95\%$. The upper figure is population of 2-level system and the line (–) is by the analytical solution, and points (×) are by the RK4 method. The lower figure is the error of the amplitude in 2-level system. The thin line is errors for the amplitude of real part, and the thick line is of imagine part.

Finally, the probability for $|1s>$ excitating to $|2p>$ calculated by numerically is about 17.82%.

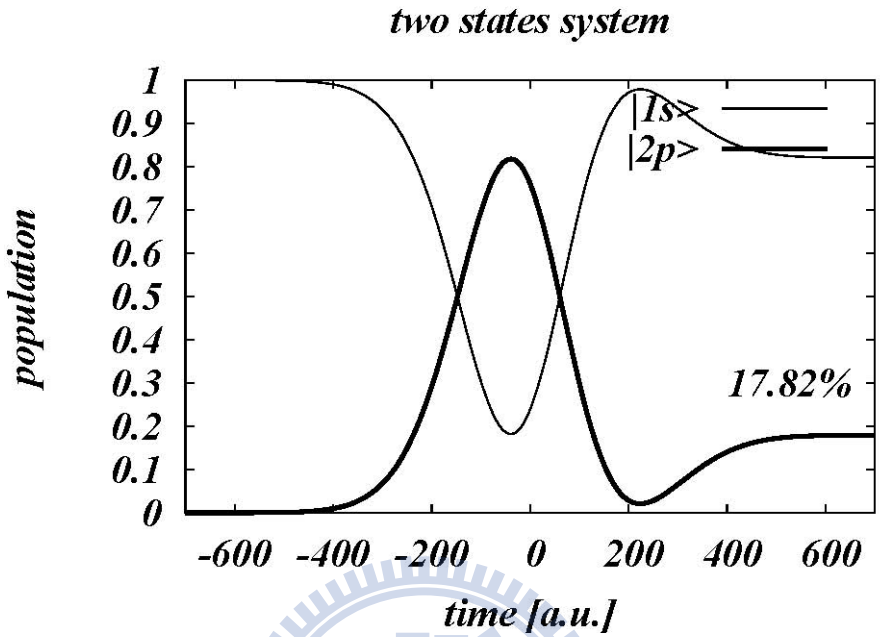

Figure. 3.5 The thin line is the population of the |1s> state, and the other one is of the $|2p>$ state. Finally, the probability of finding the electron at $|2p>$ is about 17.82% . The peak intensity and FWHM of pump APT pulse laser is respectively 2.3×10^{13} W/cm^2 and 8.5 fs.

3.2 1st order time dependent perturbation theory

When the applied electric field is not very strong, we can calculate the ionization probability by using the 1st time dependent perturbation theory. The amplitude by 1st time dependent perturbation theory is

$$C_{n\to\vec{k}}(t) = -\frac{i}{\hbar}\int_0^t e^{i(\varepsilon_k-\varepsilon_n)}\cdot <\vec{k}\,|\,H'\,|\,n>\,dt$$

$$|\vec{k}>=\sum_{l=0}\sum_{m=-l}^{l} i^l e^{-i(\sigma_l)}\cdot\frac{F_l(kr)}{r}\cdot Y^*{}_{lm}(\Omega_k)Y_{lm}(\Omega_r) \tag{3.18}$$

where $|k>$ is the continuum (unbounded) state with eigenenergy ε_k and momentum k, the $|n>$ is the bounded state with eigenenergy E_n, the Ω_k is the angle for photoelectron and the σ_l is the phase shift due to coulomb potential. In the pump probe model, we use the 1st time dependent perturbation theory to calculate the probability density for electron ionizing respectively from $|1s>$ and $|2p>$ to the unbounded state $|k>$.

Here, we use the CPC's (computer physics communication) program [4] to construct the continuum wave equation $F_l(kr)$. For checking the continuum wave equation, try to compare the continuum wave equation to the electron asymptotic wave equation at far distance between the neutron

$$\frac{F_l(kr)}{r}\xrightarrow{kr\to\infty}\frac{1}{r}\sqrt{\frac{2}{\pi k}}\sin(kr-\frac{l\pi}{2}-\gamma\ln 2kr+\sigma_l) \tag{3.19}$$

where $\gamma=-\frac{1}{k}$ for hydrogen atom. Fig. 3.6 is the result for the continuum wave function of CPC's program comparing to asymptotic form.

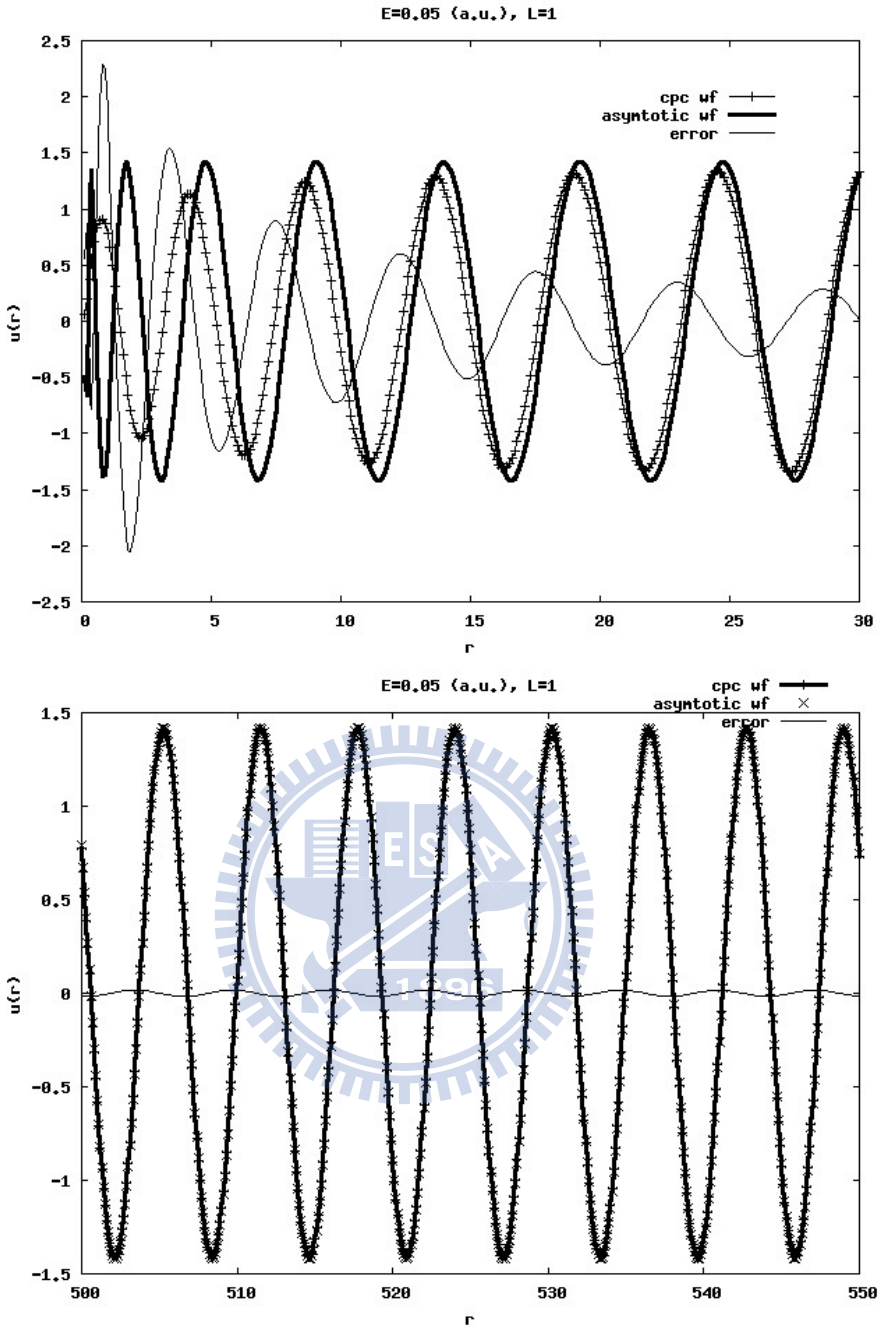

Figure. 3.6 The upper figure is about radius from 0 to 30 (a.u.) at photon energy ε_k = 0.05 (a.u.). The errors of the lower figure is bigger then upper one at the short distance between the neutron, but when the radial distance is enough to neglect Coulomb potential of hydrogen atom, the continuum wave function $|k>$ can be well identify with asymptotic wave function together.

There is still one thing that we should care about the Eqs. (3.18) starting at t = 0. In pump probe model , the pump pulse comes into the system at t = $-\tau_X/2$, so we have to modify the amplitude of 1st time dependent perturbation. To redrive the Eqs. (3.18) will contribute the phase shift about $e^{i(\varepsilon_k-\varepsilon_n)\cdot\frac{\tau_X}{2}}$, as showed in Eqs. (3.23). The wave function is the superposition of eigenstate $|n>$

$$|\Psi(t)>=\sum_n C_n(t)e^{-i\varepsilon_n(t+\frac{\tau_x}{2})}|n> \tag{3.20}$$

and the time dependent $Schrödinger$ equation is

$$\begin{aligned} & i\hbar\frac{d}{dt}|\Psi(t)>=[\hat{H}_0+H']|\Psi(t)> \\ & \Rightarrow i\hbar\sum_n[\frac{dC_n(t)}{dt}e^{-i\varepsilon_n(t+\frac{\tau_x}{2})}|n>+(-i\varepsilon_n)C_n(t)e^{-i\varepsilon_n(t+\frac{\tau_x}{2})}|n>] \\ & =\sum_n\ [C_n(t)e^{-i\varepsilon_n(t+\frac{\tau_x}{2})}\varepsilon_n|n>+e^{-i\varepsilon_n(t+\frac{\tau_x}{2})}\varepsilon_n H'|n>] \end{aligned} \tag{3.21}$$

Expand $C_n(t)$ in perturbation series

$$C_n(t)=C_n^{(0)}(t)+C_n^{(1)}(t)+\cdots \tag{3.22}$$

To intergrate the above Eqs. (3.21) will contribute a phase shift to probability amplitude

$$\begin{aligned} C^{(1)}{}_{n\to k}(t) &= \frac{-i}{\hbar}\int_{-\frac{T}{2}}^{t} e^{i(\varepsilon_k-\varepsilon_n)(t'+\frac{\tau_x}{2})}<k|H'|n>dt' \\ &= \frac{-i}{\hbar}e^{i(\varepsilon_k-\varepsilon_n)(\frac{\tau_x}{2})}\int_{-\frac{T}{2}}^{t} e^{i(\varepsilon_k-\varepsilon_n)(t')}<k|H'|n>dt' \end{aligned} \tag{3.23}$$

The formula of Eqs. (3.18) is modified to Eqs. (3.23) with accumulating the phase

$e^{i(\varepsilon_k-\varepsilon_n)\cdot\frac{\tau_x}{2}}$. The form of APT pulse for some high-harmonic order frequency which can ionizes the electron to continuum state is

$$H'_{pump}=E(t)\cdot\hat{z}=\hat{z}\cdot E_m\cdot\exp[-2\ln 2(t/\tau_x)^2]\cdot\cos(\omega t+\phi_X) \tag{3.24}$$

In pump probe model, we have to calculate $C^{(1)}{}_{1s\to k}(t)$ and $C^{(1)}{}_{2p\to k}(t)$. For the hydrogen atom , the ground state $|1s>$ is

$$\begin{aligned}|1s>&=R_{10}Y_{00}\\&=\left\{(\frac{1}{a_0})^{3/2}2e^{-r/a_0}\right\}\left\{\frac{1}{\sqrt{4\pi}}\right\}\end{aligned} \tag{3.25}$$

Here we use the atomic unit, so the $|1s>$ is

$$|1s>=\left\{2e^{-r}\right\}\left\{\frac{1}{\sqrt{4\pi}}\right\} \tag{3.26}$$

The transition amplitude from $|1s>$ to $|k>$

$$\begin{aligned}C^{(1)}{}_{1s\to k}(\frac{\tau_x}{2})&=-ie^{i(\varepsilon_k-\varepsilon_n)(\frac{\tau x}{2})}\int_{-\tau x/2}^{\tau x/2}e^{i(\varepsilon_k-\varepsilon_{1s})(t')}<k|H'_{pump}|1s>dt'\\&=-ie^{i(\varepsilon_k-\varepsilon_{1s})(\frac{\tau x}{2})}E_m\cdot<k|z|1s>\int_{-\tau x/2}^{\tau x/2}e^{i(\varepsilon_k-\varepsilon_n)(t')}e^{-2\ln 2(t/\tau x)^2}\cdot\cos(\omega t+\phi_x)dt'\\&=-ie^{i(\varepsilon_k-\varepsilon_{1s})(\frac{\tau x}{2})}E_m\cdot<k|z|1s>\left\{\frac{1}{2}e^{-i\varphi_x}e^{\frac{-[\omega-(\varepsilon_k-E_{1s})]^2}{4a}}\sqrt{\frac{\pi}{a}}\right\}\end{aligned} \tag{3.27}$$

where the $<k|z|1s>$ is the dipole matrix element which can be calculated by the numerical method, a is $2\ln 2/\tau_X{}^2$ for the electric Gaussian pulse, and here we fix the $\phi_X=0$. The dipole moment is derived to

$$
\begin{aligned}
&< k \mid z \mid 1s >=< k \mid r\cos\theta \mid 1s > \\
&= \sum_{l,m} (-i)^l e^{i\sigma_l} Y_{lm}(\Omega_k) \int dr \cdot r^3 \frac{F_l^*(kr)}{r} R_{10} \cdot \int d\Omega_r Y^*_{lm} \cdot \cos\theta \cdot Y_{00} \\
&= \frac{(-i)}{\sqrt{3}} e^{i\sigma_1} Y_{10}(\Omega_k) \int dr \cdot r^2 F_l^*(kr) R_{10}
\end{aligned}
\tag{3.28}
$$

so the transition amplitude finally becomes

$$
C^{(1)}{}_{1s\to k} = A_x \exp(i\varphi_x) \cdot Y_{10}(\Omega_k) \tag{3.29}
$$

where

$$
\begin{aligned}
A_x &= -\frac{1}{\sqrt{3}} E_m \cdot \left\{ e^{\frac{-[\omega - (\varepsilon_k - E_{1s})]^2}{4a}} \sqrt{\frac{\pi}{a}} \right\} \left(\int dr \cdot r^2 F_l^*(kr) R_{10} \right) \\
\varphi_x &= (\varepsilon_k - E_{1s}) \left(\frac{\tau_x}{2} \right) + \sigma_1 - \phi_X
\end{aligned}
\tag{3.30}
$$

For the second path from $|2p>$ to $|k>$, the probe IR laser pulse is used to

$$
H'_{probe} = E(t)\hat{\varepsilon} \cdot \hat{r} = \hat{\varepsilon} \cdot \hat{r} \cdot E_0 \cdot \exp[-2\ln 2(t - \tau / \tau_L)^2] \cdot \cos[\ \omega(t-\tau) + \varphi_L\ ]
$$

where the E_0 is the maximum amplitude, $\hat{\varepsilon} \cdot \hat{r}$ is the direction, τ_L is the duration time and the CEP of IR lasse pulse φ_L = -π/2. Secondly, to calculate the transition amplitude from $|2p>$ state to the $|k>$

$$
\begin{aligned}
C^{(1)}{}_{2p\to k}\left(\frac{\tau_L}{2}\right) &= -ie^{i(\varepsilon_k - \varepsilon_n)\left(\frac{\tau_L}{2}\right)} \int_{-\tau_L/2}^{\tau_L/2} e^{i(\varepsilon_k - \varepsilon_{2p})(t')} < k \mid H'_{probe} \mid 2p > dt' \\
&= -ie^{i(\varepsilon_k - \varepsilon_{2p})\left(\frac{\tau_L}{2}\right)} E_0 \cdot < k \mid \hat{\varepsilon} \cdot \hat{r} \mid 2p > \left\{ \frac{1}{2} e^{-i\varphi_L} e^{\frac{-[\omega - (\varepsilon_k - E_{2p})]^2}{4a'}} \sqrt{\frac{\pi}{a'}} \right\}
\end{aligned}
\tag{3.31}
$$

Here, to control the probe IR laser pulse's direction, we expand the $\hat{\varepsilon}\cdot\vec{r}$ to

$$\hat{\varepsilon}\cdot\vec{r} = r\{\ \frac{4\pi}{3}[\ Y^*_{1,-1}(\theta_l,\varphi_l)Y_{1,-1}(\theta,\varphi)+Y^*_{1,0}(\theta_l,\varphi_l)Y_{1,0}(\theta,\varphi) + Y^*_{1,1}(\theta_l,\varphi_l)Y_{1,1}(\theta,\varphi)\ ]\ \} \tag{3.32}$$

where the θ_l is the polar angle and φ_l azimuth angle of the direction of probe laser. Futnermore, the radial part in the Eqs. (3.31) becomes

$$\begin{aligned} <k\mid\hat{\varepsilon}\cdot\hat{r}\mid 2p>= &-\frac{1}{\sqrt{10}}\sin(\theta_l)\cdot e^{i\sigma_2}\cdot <F_2\cdot R_{21}>Y_{2,-1}(\Omega_k)\int dr\cdot r^2F_2^*(kr)R_{21} \\ &-\sqrt{\frac{4}{15}}\cos(\theta_l)\cdot e^{i\sigma_2}\cdot Y_{2,0}(\Omega_k)\int dr\cdot r^2F_2^*(kr)R_{21} \\ &+\frac{1}{\sqrt{10}}\cos(\theta_l)\cdot e^{i\sigma_2}\cdot Y_{2,1}(\Omega_k)\int dr\cdot r^2F_2^*(kr)R_{21} \\ &-\sqrt{\frac{1}{3}}\sin(\theta_l)\cdot e^{i\sigma_0}\cdot Y_{0,0}(\Omega_k)\int dr\cdot r^2F_0^*(kr)R_{21} \end{aligned} \tag{3.33}$$

Here we fix the $\varphi_l = 0$. Finally, deduce the transition amplitude for the second path to

$$\begin{aligned} M_{if}(\theta_l,\varphi_l) = &\ a_1e^{i\varphi_1}\{\ Y^*_{1,-1}(\Omega_l)Y_{2,-1}(\Omega_k)+Y^*_{1,1}(\Omega_l)Y_{2,1}(\Omega_k)\ \} \\ &+\{\ a_2e^{i\varphi_1}Y_{2,0}(\Omega_k)+a_3e^{i\varphi_2}Y_{0,0}(\Omega_k)\ \}\sqrt{\frac{3}{4\pi}}\cos\theta_l \\ &+be^{i\varphi_b}Y_{1,0}(\Omega_k) \end{aligned} \tag{3.34}$$

where

$$\begin{aligned} a_1 &= \frac{E_0}{2}\exp\{\ \frac{[\omega_{probe}-(\varepsilon_k-E_{2p})]^2}{8\ln 2/\tau_L^{\ 2}}\ \}\sqrt{\frac{\pi\tau_L^{\ 2}}{2\ln 2}}\mid M_{2p,1s}\mid\sqrt{\frac{4\pi}{15}}\cdot\int r^2F_2^{\ *}R_{21}dr \\ a_2 &= \frac{E_0}{2}\exp\{\ \frac{[\omega_{probe}-(\varepsilon_k-E_{2p})]^2}{8\ln 2/\tau_L^{\ 2}}\ \}\sqrt{\frac{\pi\tau_L^{\ 2}}{2\ln 2}}\mid M_{2p,1s}\mid\frac{3}{4}\sqrt{\frac{\pi}{5}}\cdot\int r^2F_2^{\ *}R_{21}dr \\ a_3 &= \frac{E_0}{2}\exp\{\ \frac{[\omega_{probe}-(\varepsilon_k-E_{2p})]^2}{8\ln 2/\tau_L^{\ 2}}\ \}\sqrt{\frac{\pi\tau_L^{\ 2}}{2\ln 2}}\mid M_{2p,1s}\mid\frac{2}{3}\sqrt{\pi}\cdot\int r^2F_0^{\ *}R_{21}dr \\ b &= -\frac{E_m}{2}\exp\{\ \frac{[\omega_{pump}-(\varepsilon_k-E_{1s})]^2}{8\ln 2/\tau_x^{\ 2}}\ \}\sqrt{\frac{\pi\tau_x^{\ 2}}{2\ln 2}}\cdot\int r^2F_1^{\ *}R_{10}dr \end{aligned} \tag{3.35}$$

$$\varphi_1 = \phi_{p,s} - t_d E_{2p} + \sigma_2 + (\varepsilon_k - E_{2p})\frac{\tau_L}{2} - \varphi_L - \frac{\pi}{2}$$
$$\varphi_2 = \phi_{p,s} - t_d E_{2p} + \sigma_0 + (\varepsilon_k - E_{2p})\frac{\tau_L}{2} - \varphi_L - \frac{\pi}{2} \qquad (3.36)$$
$$\varphi_b = (\varepsilon_k - E_{1s})\frac{\tau_X}{2} - \phi_X + \sigma_1 - (t_d\varepsilon_k + \tau_L\varepsilon_k + \vec{\alpha}\cdot\vec{k} + \beta)$$

It is a little complication to derive the equation. If you have patience, there are some information in Eqs. (3.34). For different direction between probe IR pulse and APT pulse, there are $Y_{2,-1}(\Omega_k)$ and $Y_{2,1}(\Omega_k)$ contribute on the transition amplitude and break the symmetry on azimuth angle. The localization of photon is different for the linea polarization effect, because the $Y_{2,-1}(\Omega_k)$ and $Y_{2,1}(\Omega_k)$ contribute on the transition amplitude.

To integrate the transition angle-resolved probability density for whole photoelectron angle can get energy spectrum P_ε

$$P_\varepsilon = P_\varepsilon(\varepsilon_k) = \frac{dP}{d\varepsilon} = \int |M_{if}|^2 \, d\Omega_k$$
$$= a_1^{\,2}\left(|Y_{1,-1}(\Omega_l)|^2 + |Y_{1,1}(\Omega_l)|^2 \right) + \left(a_2^{\,2} + a_3^{\,2} \right) |Y_{1,0}(\Omega_l)|^2 + b^2 \qquad (3.37)$$

From Eqs. (3.37), find that the P_ε is not dependent on the time delay t_d, so the total ionization probability P is too.

$$P = \int d\varepsilon_k \int |M_{if}|^2 \, d\Omega_k \qquad (3.38)$$

3.3 Numerical result

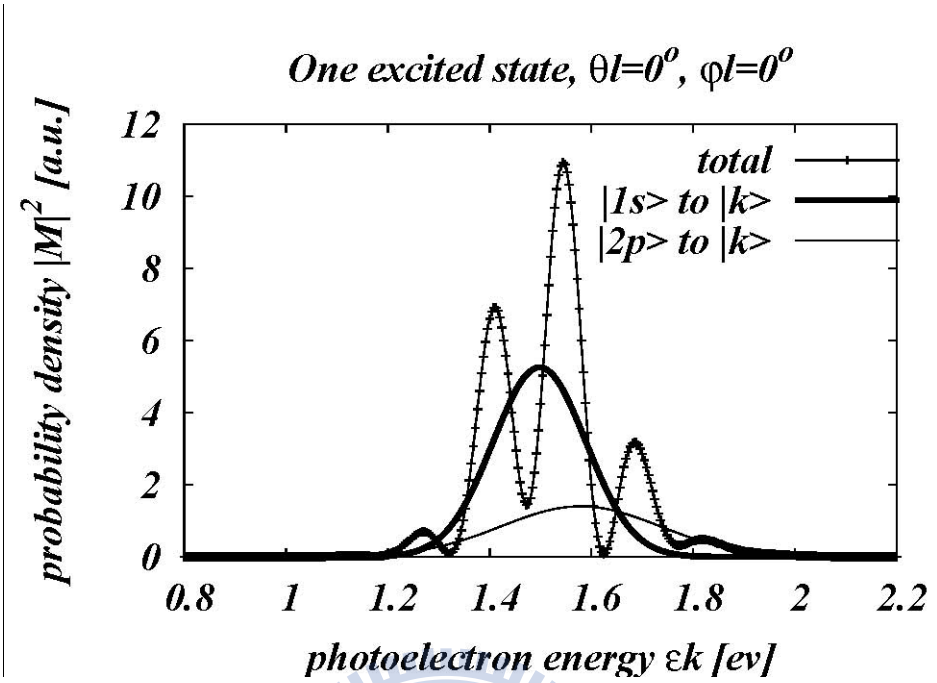

Figure. 3.7 Photoelectron energy spectrum $|M_{if}(t)|^2$ (line-points) obtained by computing the Eqs. (3.8) in pump-probe model (two-path interference model) at the specific momentum direction θ_k = 0.314159, the time delay t_d = 7fs and the direction of IR laser pulse aligning to parallel to z axis. The thick line and thin line are respectively the $|M_{k,1s}|^2$ and $|M_{k,2p}|^2 |M_{2p,1s}|^2$. The peak intensity of pump and probe laser is 2.3×10^{13} and 2.0×10^{13} W/cm^2, and the FWHM of pump and probe laser is 8.5 and 9 fs.

From the Eqs. (3.8), when the photoelectron angle θ_k and linear polarization direction being fixed, we assumed the variables Φ are constant in Eqs. (3.8) when the time delay t_d changes, and the we can find when the

$$(\varepsilon_k - E_{2p}) \cdot t_d = 2\pi \cdot n$$

where n is a positive or negative integer, the fringe will be a hyperbolic structure in the transition probability density. You also can see the structure in experimental data by [5].

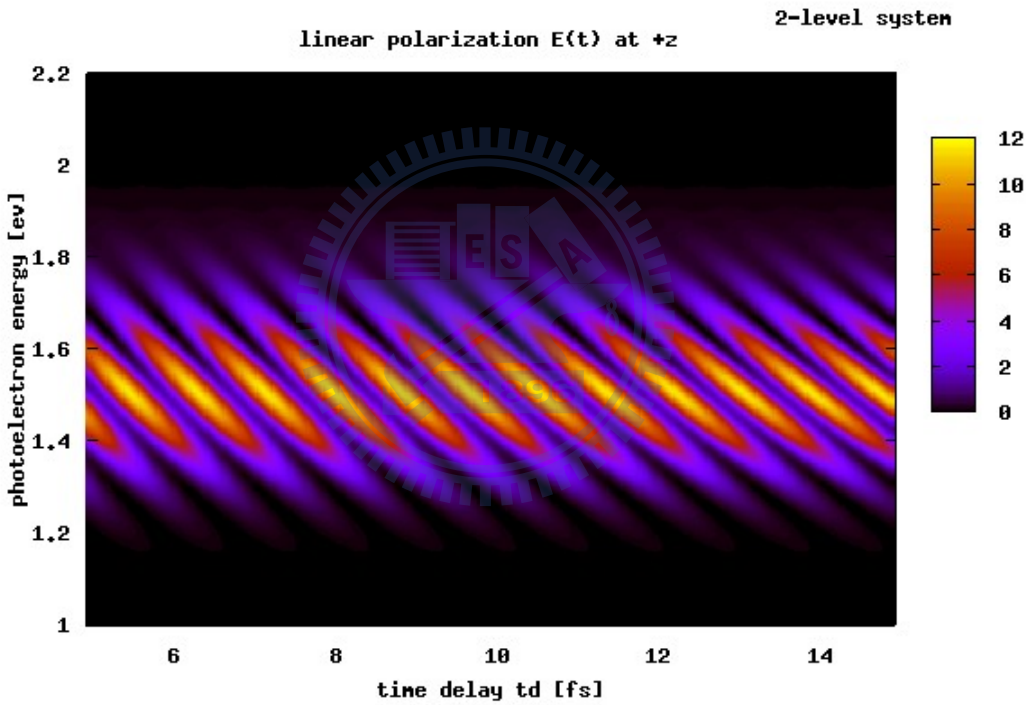

Figure. 3.8 The transition probability density $|M_{if}|^2$ depdents on photoelectron energy ε_k and the time delay t_d.

Chapter 4.

Considering two excited states in pump-probe model

For adding one more unbounded state, we choose the third and fourth excited state of hydrogen atom as two unbounded state, and simulate four high-harmonics orders in APT pulse. There are two unbounded state and a continuum state as intermediate state. Derive the transition probability amplitude as

$$M_{if} = e^{-iE_{3p}t_d} M_{k,3p} M_{3p,1s} + e^{-iE_{4p}t_d} M_{k,4p} M_{4p,1s} + e^{-i\varepsilon_k t_d} e^{-i(\tau_L \cdot \varepsilon_k + \vec{\alpha}\cdot\vec{k}+\beta)} M_{k,1s} \tag{4.1}$$

To use the Fig. 4.1 to describe the mechanism for considering two excited states in pump-probe model

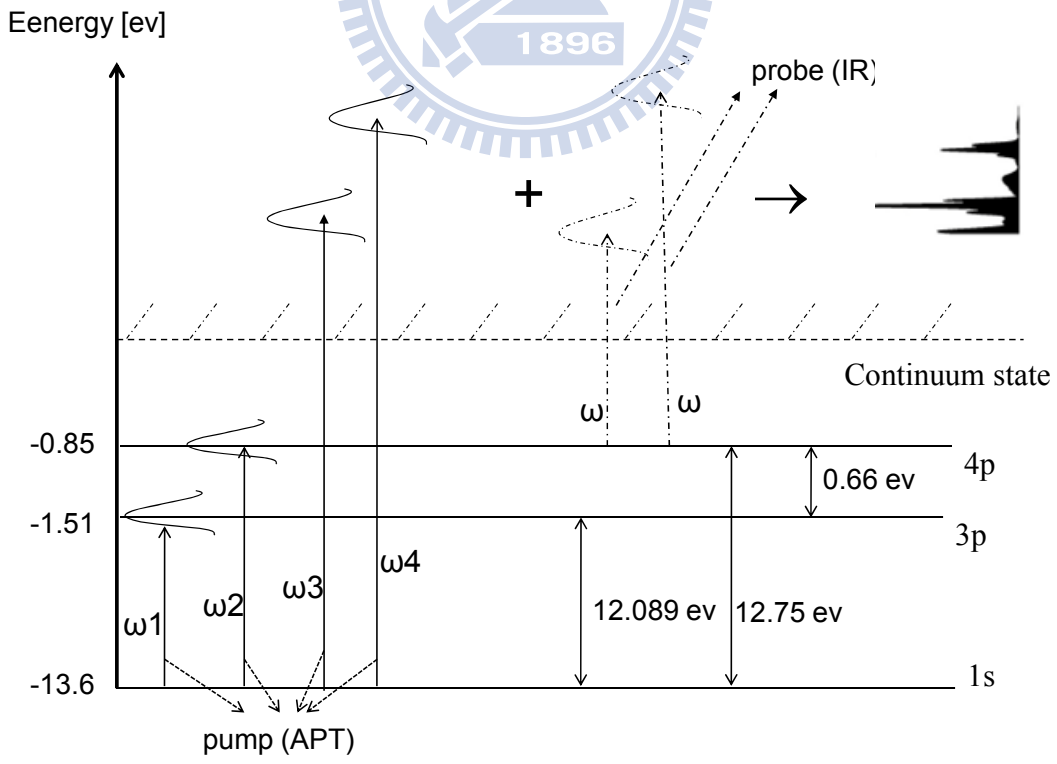

Figure. 4.1 ω1=11.95 ev, ω2=12.67 ev, ω3=16.3ev, ω4=17.1 ev, ω=4.3 ev

From the Fig. 4.1, APT contains four pulses: two pulses respectively contribute the probability for pumping an electron respectively to the $|3p>$ and $|4p>$, and other pulses give the probability for ionizing an electron to the continuum state. After time delay t_d, the probe laser pulse coming into the system is called the second path, and contributes the probability for ionizing the electron from $|3p>$ and $|4p>$ respectively to continuum state and then interfere with the wave packets by first path which is by the APT pulse.

Like considering one excited state in pump-probe model, to see clarity the magnitudes and phases in the transition probability amplitude, we define that

$$\begin{cases} M_{k,3p} = c_{3p}\exp(i\phi_{3p}) \\ M_{k,4p} = c_{4p}\exp(i\phi_{4p}) \\ M_{k,1s} = c_{1s}\exp(i\phi_{1s}) \end{cases} \qquad \begin{cases} M_{3p,1s} = a_{3p}\exp(i\varphi_{3p}) \\ M_{4p,1s} = a_{4p}\exp(i\varphi_{4p}) \end{cases} \tag{4.2}$$

Finally, the ionization probability density for two excited state in pump probe model is expressed clearly as

$$\begin{aligned} |M_{if}|^2 = {} & c_{1s}{}^2 + a_{3p}{}^2 c_{3p}{}^2 + a_{4p}{}^2 c_{4p}{}^2 \\ & + 2a_{3p}a_{4p}c_{3p}c_{4p}\cos\left[(\varphi_{3p}+\phi_{3p}) - (\varphi_{4p}+\phi_{4p}) - (E_{3p}-E_{4p})t_d \right] \\ & + 2a_{3p}c_{3p}c_{1s}\cos\left[(\phi_{1s}-\varphi_{3p}-\phi_{3p}) - (\tau_L\varepsilon_k + \vec{\alpha}\cdot\vec{k} + \beta) - (\varepsilon_k - E_{3p})t_d \right] \\ & + 2a_{4p}c_{4p}c_{1s}\cos\left[(\phi_{1s}-\varphi_{4p}-\phi_{4p}) - (\tau_L\varepsilon_k + \vec{\alpha}\cdot\vec{k} + \beta) - (\varepsilon_k - E_{4p})t_d \right] \end{aligned} \tag{4.3}$$

In RHS (right hand side) of Eqs. (4.3) , the first term is contributed by the first path which gives the probability of an electron ionizing to the continuum states by pump APT pulse, and the second and third term are contributed by the second path that produces the probability of an electron exciting to the $|3p>$ and $|4p>$ by APT pulse and then ionizing

from $|3p>$ and $|4p>$ respectively to the continuum state with the same momentum as the first path by the probe IR pulse. The first and the second path interfering with each other in the same photoelectron momentum k gives rise to the others term which are all dependent on the time delay t_d. We redrive the Eqs. (4.3) to the other form dependent on photoelectron angle θ_k

$$\begin{aligned} M_{if} =& |M_{3p,1s}| \{ A_{3p}e^{i\delta_1}Y_{2,-1}(\Omega_k) + B_{3p}e^{i\delta_1}Y_{2,1}(\Omega_k) + C_{3p}e^{i\delta_1}Y_{2,0}(\Omega_k) + D_{3p}e^{i\delta_2}Y_{0,0}(\Omega_k) \} \\ &+ |M_{4p,1s}| \{ A_{4p}e^{i\eta_1}Y_{2,-1}(\Omega_k) + B_{4p}e^{i\eta_1}Y_{2,1}(\Omega_k) + C_{4p}e^{i\eta_1}Y_{2,0}(\Omega_k) + D_{4p}e^{i\eta_2}Y_{0,0}(\Omega_k) \\ &+ E_{1s}e^{-i\beta_{1s}}Y_{1,0}(\Omega_k) \end{aligned} \tag{4.4}$$

where the coefficients are showed in Appendix A.

To integrate the transition angle-resolved probability density over photoelectron angle can find that the phase of the energy-resolved probability density P_ε depdentent on the time delay t_d is about $(E_{4p} - E_{3p})t_d$, so the P_ε will change with time delay t_d and the frequency is $\frac{2\pi}{(E_{4p} - E_{3p})}$ ≈ 6.26 fs , as showed in Eqs. (4.5) and Fig. 4.6.

$$\begin{aligned} P_\varepsilon = P_\varepsilon(\varepsilon_k) &= \frac{dP}{d\varepsilon} = \int |M_{if}|^2 \, d\Omega_k \\ &= A_{3p}{}^2 + B_{3p}{}^2 + C_{3p}{}^2 + D_{3p}{}^2 + A_{4p}{}^2 + B_{4p}{}^2 + C_{4p}{}^2 + D_{4p}{}^2 + E_{1s}{}^2 \\ &+ 2\left(A_{3p}A_{4p} + B_{3p}B_{4p} + C_{3p}C_{4p} \right) \times |M_{3p,1s}||M_{4p,1s}| \cos(\eta_1 - \delta_1) \\ &+ 2D_{3p}D_{4p} \times |M_{3p,1s}||M_{4p,1s}| \cos(\eta_2 - \delta_2) \end{aligned} \tag{4.5}$$

On the other hand, the probability P maybe has the same frequency with energy spectrum P_ε for dependence on time delay, as showed in Fig. 4. 7.

4.1 Three-level system

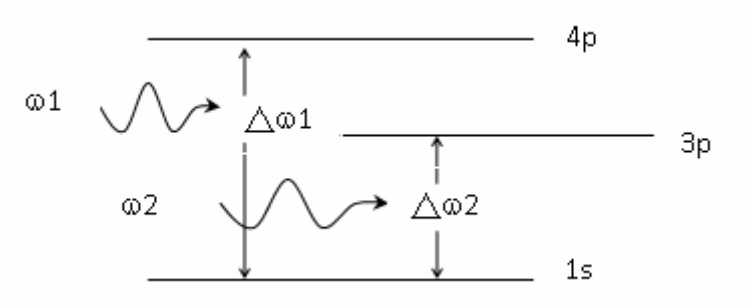

Figure. 4.2 △ω1=12.75 ev, △ω2=12.089 ev, ω1=11.95 ev and ω2=12.67 ev

For considering one more excitation state, the wave function become the superposition of hydrogen atom's eigenstate $|1s>$, $|3p>$ and $|4p>$

$$|\Psi(t)>= c_{1s}(t)e^{-i\hbar\omega_{1s}t}(t)\,|1s>+c_{3p}(t)e^{-i\hbar\omega_{3p}t}\,|3p>+c_{4p}(t)e^{-i\hbar\omega_{4p}t}\,|4p> \quad (4.7)$$

where $\hbar\,\omega_{1s}$, $\hbar\,\omega_{3p}$ and $\hbar\,\omega_{4p}$ are respectively the eigenenergy of $|1s>$, $|3p>$ and $|4p>$ for hydrogen atom, and the $C_{1s}(t)$, $C_{3p}(t)$ and $C_{4p}(t)$ are the probability amplitude of finding the electron in states $|1s>$, $|3p>$ and $|4p>$

The external electric field contains four pulse in pump APT pulse, but only two pulse is respectively nearly resonant to the frequency for $|1s>$ to $|3p>$ and $|1s>$ to $|4p>$. Put the Eqs. (4.7) into the time-dependent *Schrödinger* equation, so we can write down the three ordinary differential equations as

$$i\dot{c}_{1s}(t)=\frac{E_m}{2}\cdot\left[\; e^{i(\omega 1-\Delta\omega 1)t}<1s\,|\,z\,|\,4p>c_{4p}(t)+e^{i(\omega 2-\Delta\omega 2)t}<1s\,|\,z\,|\,3p>c_{3p}(t)\;\right]$$

$$i\dot{c}_{3p}(t)=\frac{E_m}{2}\cdot e^{-i(\omega 2-\Delta\omega 2)t}<3p\,|\,z\,|\,1s>c_{1s}(t)$$

$$i\dot{c}_{4p}(t)=\frac{E_m}{2}\cdot e^{-i(\omega 1-\Delta\omega 1)t}<4p\,|\,z\,|\,1s>c_{1s}(t)$$

(4.5)

where E_m is peak value of the pump APT pulse, and $<1s|z|4p>$ and $<1s|z|3p>$ are the dipole moment. To carry on checking my program, we use the electric field as

$$H' = E(t)\cdot\hat{z} = \hat{z}\cdot E_m \cdot \cos(\omega t + \varphi) \tag{4.6}$$

to check my program and there are analytical solutions for resonant frequency[3].

$$\begin{cases} c_{1s} = \cos(\dfrac{\Omega t}{2}) \\ c_{3p} = \dfrac{\Omega^*_{R1}}{\Omega}\sin(\dfrac{\Omega t}{2}) \\ c_{4p} = \dfrac{\Omega^*_{R2}}{\Omega}\sin(\dfrac{\Omega t}{2}) \end{cases}$$

$$\begin{aligned} \Omega_{R1} &= <1s|z|3p>\cdot Em \\ \Omega_{R2} &= <1s|z|4p>\cdot Em \\ \Omega^2 &= \Omega_{R1}{}^2 + \Omega_{R2}{}^2 \end{aligned} \tag{4.7}$$

Use the analytical solutions on resonant frequency to compare my numerical result for checking my RK4 program.

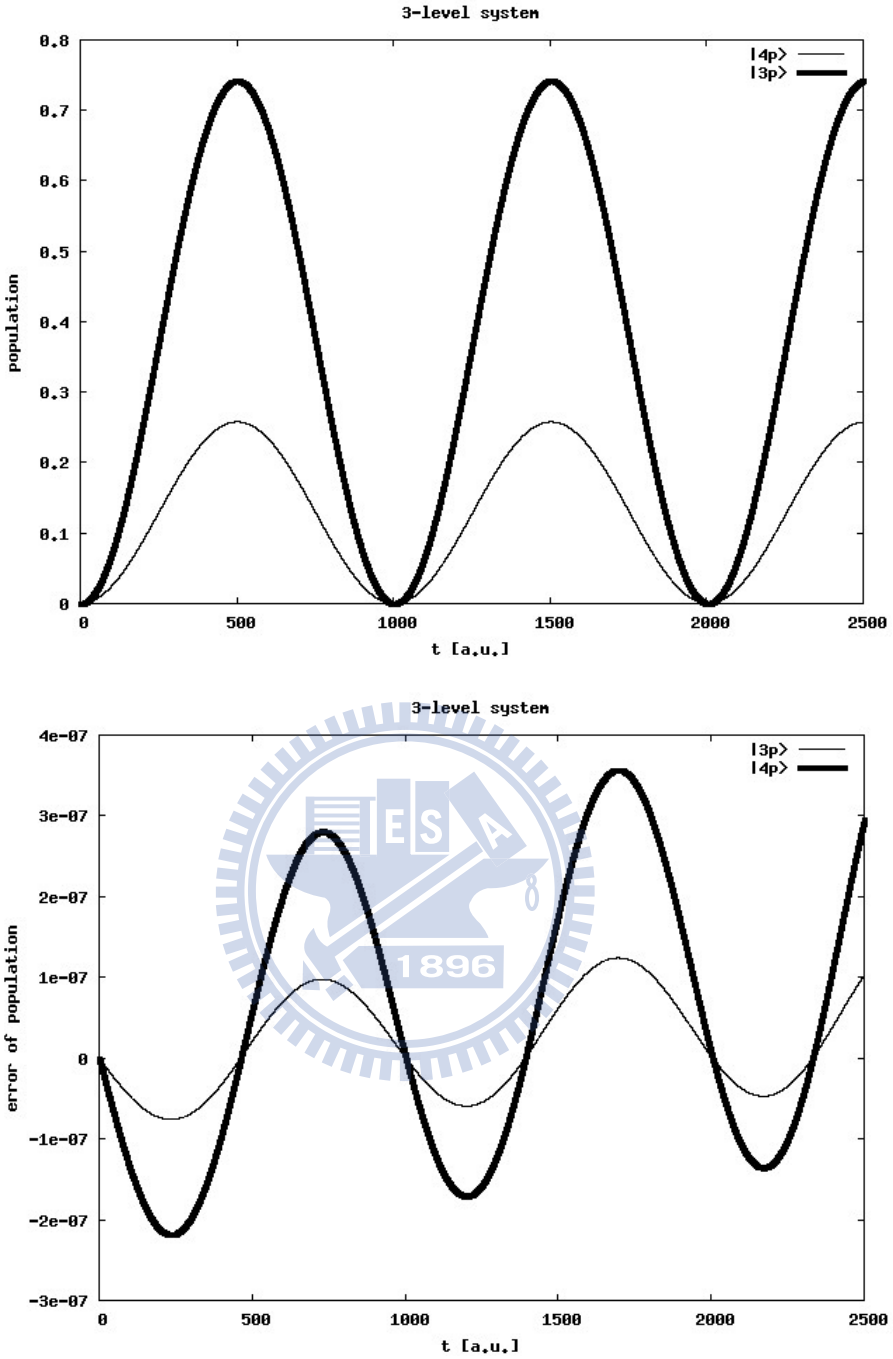

Figure. 4.3 Computing the RK4 method to compare the analytical solutions on resonant frequency, and the maximum of error is about 3.5×10^{-7}. The parameter respectively is E_0=0.018 (a.u.), $\omega 1=\triangle\omega 1$=12.75 (ev) and $\omega 2=\triangle\omega 2$=12.089 (ev)

Finally, computing the population of 3-level system for considering the Gaussian pulse shape in APT pulse is about 17.16% for $|3p>$ state and 18.87% for $|4p>$ state.

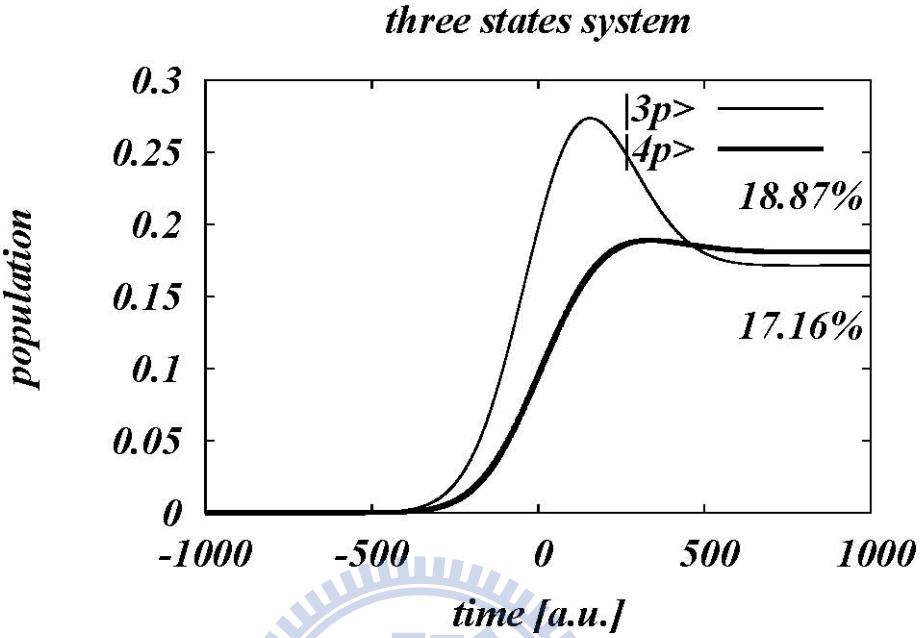

Figure. 4.4 The 3-level system in hydrogen atom. The thick line is the probability for finding electron at the $|4p>$ state and the thin line is the probability for finding the electron at the $|3p>$ state. The Peak intensity and FWHM of pump laser is 1.5×10^{13} W/cm^2 and 9 fs.

4.2 Numerical result

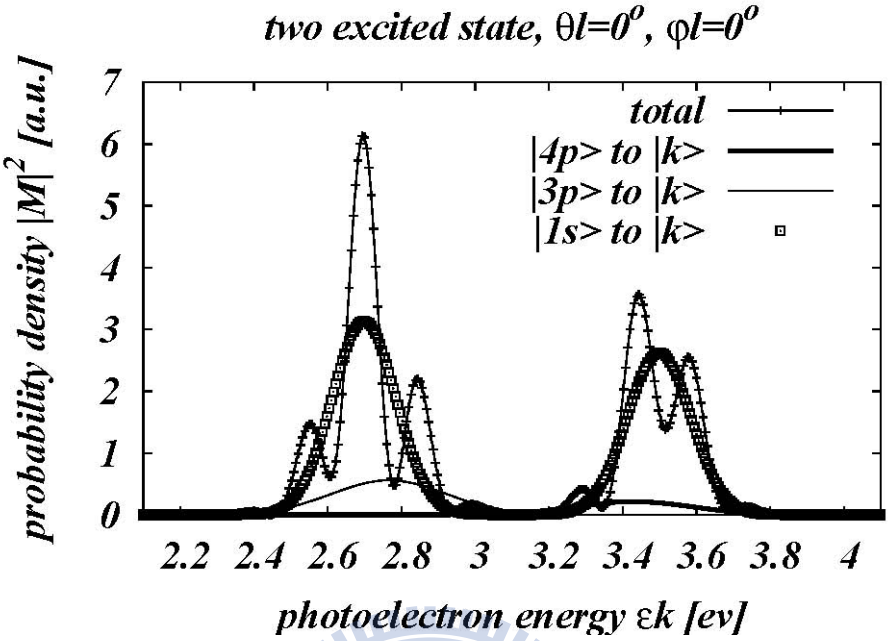

Figure. 4.5 Photoelectron angle-resolved energy spectrum $|M_{if}(t)|^2$ (line-points) for considering two excited state in pump-probe model (two-path interference model) obtained by computing the Eqs. (4.3) at the specific momentum direction $\theta_k = 3$ and the time delay $t_d = 6$fs. The thin line and thick line are respectively the $|M_{k,3p}|^2 |M_{3p,1s}|^2$ and $|M_{k,4p}|^2 |M_{4p,1s}|^2$, and the points $(\times)$ is the probability density for $|M_{k,1s}|^2$. The peak intensity of pump and probe laser is 1.5×10^{13} W/cm^2, and the FWHM of pump and probe laser is respectively 9 and 5 fs.

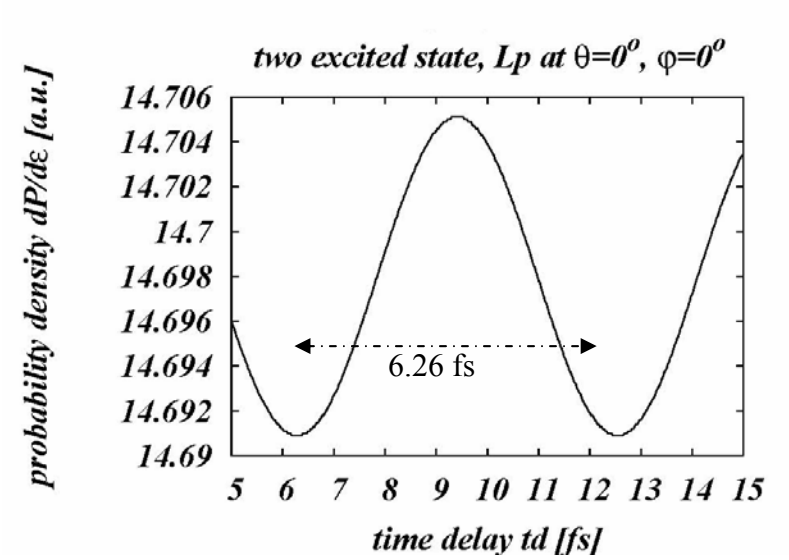

Figure. 4.6 The transition energy-resolved probability density $\frac{dP}{d\varepsilon_k}$ dependents on the time delay t_d. The different value between the maximum and minimum is very small because the interference term coming from the $M_{k,3p}$ and $M_{k,4p}$ multiplying together, but the wave packet of $M_{k,3p}$ and $M_{k,4p}$ in energy domain is not the same, and one of them will be too small at a particular photoelectron energy ε_k. Hence, the interference does not change so much.

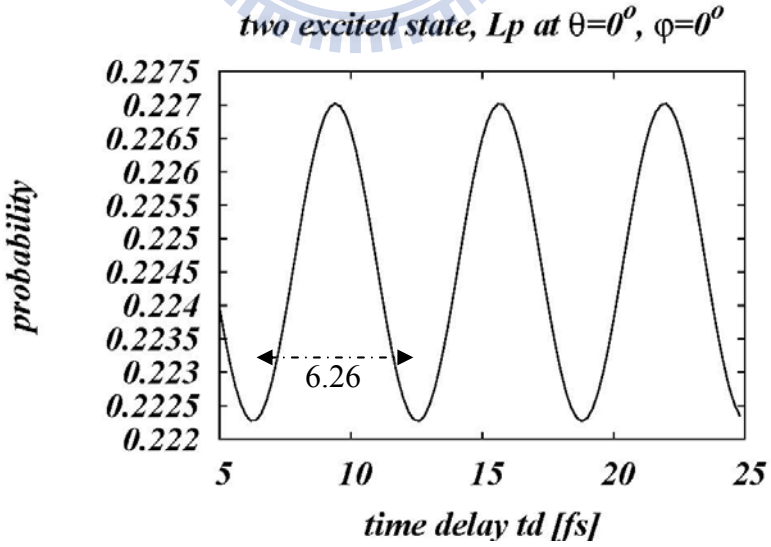

Figure. 4.7 The total ionization probability for considering two excited state in pump-probe model. The frequency of the probability P that repeats again is the same P_ε.

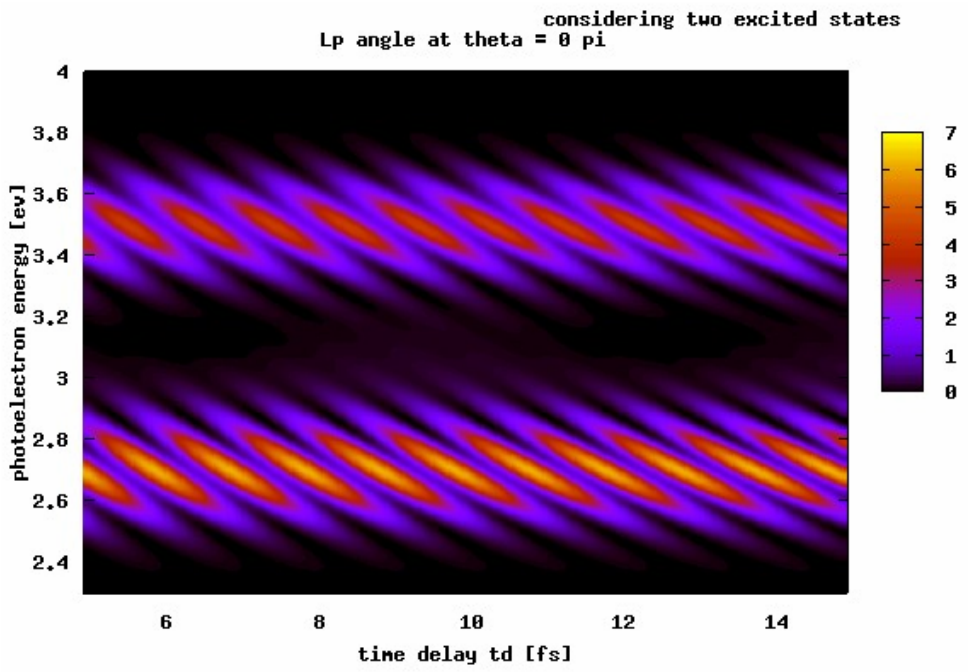

Figure. 4.8 The transition probability density $|M_{if}|^2$ for considering two excited state in pump-probe model depdents on photoelectron energy ε_k and the time delay t_d at the $\theta_k = 3$.

Chapter 5.

Linear and elliptical polarization effect

5.1 Linear polarization effects

For clarity, we consider only one excited state in pump-probe model to discuss the polarization effect. Rederive Eqs. (3.34) to

$$M_{if}(\theta_l,\varphi_l) = A_1 e^{i\alpha_1}\sin\theta_l + A_2 e^{i\alpha_2}\cos\theta_l + Be^{i\varphi_b} \tag{5.1}$$

where

$$\begin{aligned} A_1 &= a_1\frac{\sqrt{45}}{4\pi}\sin\theta_k\cos\theta_k\cos(\varphi_k-\varphi_l) \\ \alpha_1 &= \varphi_1 \\ A_2 e^{i\alpha_2} &= \sqrt{\frac{3}{4\pi}}\left\{\, a_2 e^{i\varphi_1}Y_{2,0}(\Omega_k) + a_3 e^{i\varphi_2}Y_{0,0}(\Omega_k)\,\right\} \\ B &= bY_{1,0}(\Omega_k) \end{aligned} \tag{5.2}$$

In Eqs. (5.1), if θ_l = 0, the first term on the RHS equals zero and the term of interference only comes from the 2nd term multiplying to the 3rd term which coming from the first path. However, if θ_l ≠ 0, the additional second term will comtribute to the interference effect. Expand the Eqs. (5.1) to angular-resolved probability density as

$$\begin{aligned} |M_{if}(\theta_l,\varphi_l)|^2 = {} & A_1^2\sin^2\theta_l + A_2^2\cos^2\theta_l + B^2 \\ & + A_1A_2\cos(\alpha_2-\alpha_1)\sin(2\theta_l) \\ & + 2A_1B\cos(\varphi_b-\alpha_1)\sin\theta_l \\ & + 2A_2B\cos(\varphi_b-\alpha_2)\cos\theta_l \end{aligned} \tag{5.3}$$

From Eqs. (5.3), additional terms contributing to the interference effect under the probe IR pulse without the alignment to parallel with the pump APT pulse are the $A_1A_2\cos(\alpha_2-\alpha_1)\sin(2\theta_l)$ and $2A_1B\cos(\varphi_b-\alpha_1)\sin\theta_l$, but the difference of phase, $\alpha_2-\alpha_1$,

is not dependent on the time delay t_d and only equals the $\sigma_2 - \sigma_0$ which comes from the coulomb potential phase. Furthermore, the part of the phase in the $2A_1 B\cos(\varphi_b - \alpha_1)\sin\theta_l$ which is dependent on time delay t_d is $(\varepsilon_k - E_{2p})\cdot t_d$ as the same as that in the $2A_2 B\cos(\varphi_b - \alpha_2)\cos\theta_l$, so the number of hyperbola's fringes must be the same in the time delay from t_d = 5 to 15 fs. The transition angle-resolved probability density v.s. photoelectron energy ε_k and time delay t_d is showed in Fig. 5.1.

From the Eqs. (3.34) and (5.1), the coefficient of $\sin\theta_l$ depends on the spherical harmonics $Y_{2,-1}(\Omega_k)$ and $Y_{2,1}(\Omega_k)$, and $\cos\theta_l$ depends on the spherical harmonics $Y_{2,0}(\Omega_k)$ and $Y_{0,0}(\Omega_k)$. The $Y_{2,0}(\Omega_k)$ and $Y_{0,0}(\Omega_k)$ are symmetric for rotating a random azimuth angle φ_k, but $Y_{2,-1}(\Omega_k)$ and $Y_{2,1}(\Omega_k)$ are not. The cylindrosymmetry is broken because of $Y_{2,-1}(\Omega_k)$ and $Y_{2,1}(\Omega_k)$. Fig. 5.2 is the spherical surface of the probability density at particular photoelectron energy, and the distance value from origin to the surface is the probability density. Fig. 5.2 shows that the asymmetry on azimuth angle comes from the IR laser pulse and the symmetry is broken by the phase coming from the time delay process. However, to change the direction of probe IR laser pulse can control the localization of the photoelectron, as an example showed in Fig. 5.4.

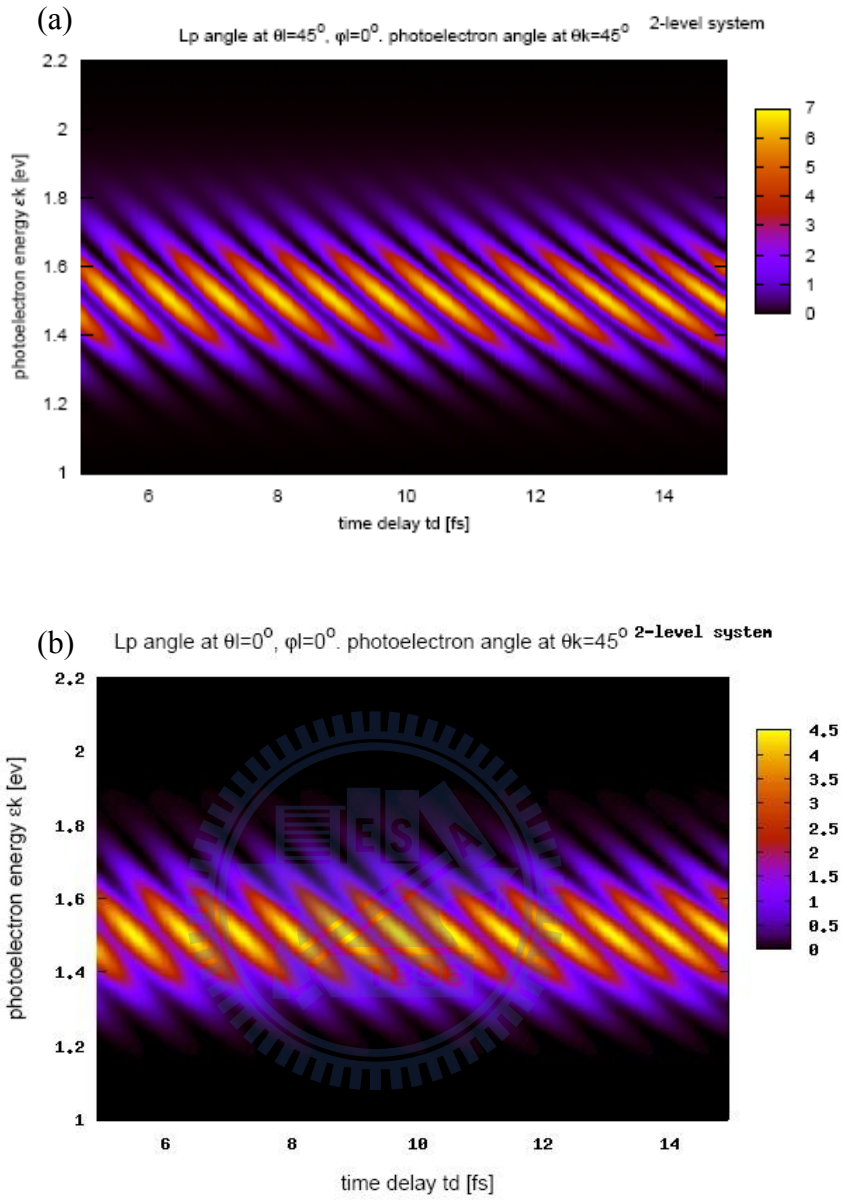

Figure. 5.1 The IR pulse is aligned at (a) $\theta_l = 45^o$ and $\varphi_l = 0^o$, (b) $\theta_l = 0^o$ and $\varphi_l = 0^o$. The number of the fringes (a) and (b) are the same in t_d from 5 to 15 fs, but the structure is not. The photoelectron angle θ_k =45°

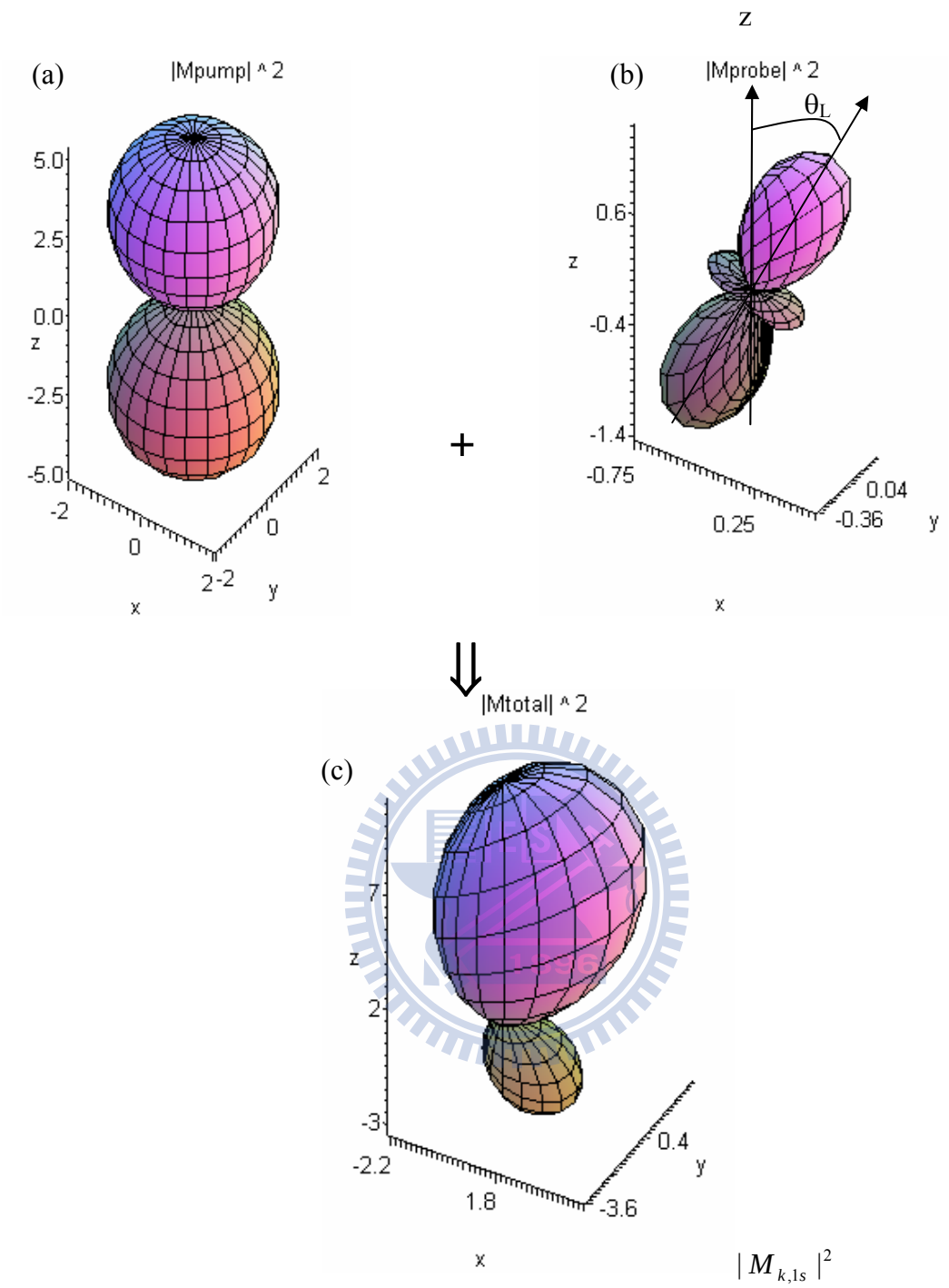

Figure. 5.2 The transition probability density for (a) first path, $|M_{k,1s}|^2$, (b) second path, $|M_{k,2p}|^2|M_{2p,1s}|^2$ and (c) total path, $|M_{if}|^2$ at assigning the direction of probe IR pulse at $\theta_l = 45^o$ and $\varphi_l = 0^o$ with time delay t_d = 7 fs and ε_k = 1.544 ev.

From Fig 5.3 and 5.4 can find that the photoelectron gets more probability desntiy to emit at angle 0^o for probe IR pulse aligned to parallel with z axis, and has the symmetry for rotating a random azimuth angle. When the IR pulse direction does not be aligned with z axis, the maximum transition probability density is different with that parallel to z axis and the symmetry on azimuth angle is broken. The maximum value of probability density for assigning the direction at $\theta_l = 45^o$ & $\varphi_l = 0$ is at $\theta_k = 14.4^o$, and $\theta_l = 90^o$ & $\varphi_l = 0$ is about $\theta_k = 27^o$ & 153^o which is symmetric at $\theta_k = 0$. When the direction at $\theta_l = 0^o$ and $\varphi_l = 0$, the probability density by first and second path is respectively symmetric on polar angle at origin, but the total transition probability density by the first path and the second path interfering with each other is not symmetric at origin. The region of photoelectron angle θ_k from 0 to $\pi/2$,which is called the left side, interfere constructively by the first path and second path, but the other side called right side interfere destructively with each other. Besides, as direction is at $\theta_l = 45^o$ & $\varphi_l = 0$, the only difference with $\theta_l = 0^o$ is the partial probability density by the second IR laser pulse, and there is no symmetry on polar angle anymore.

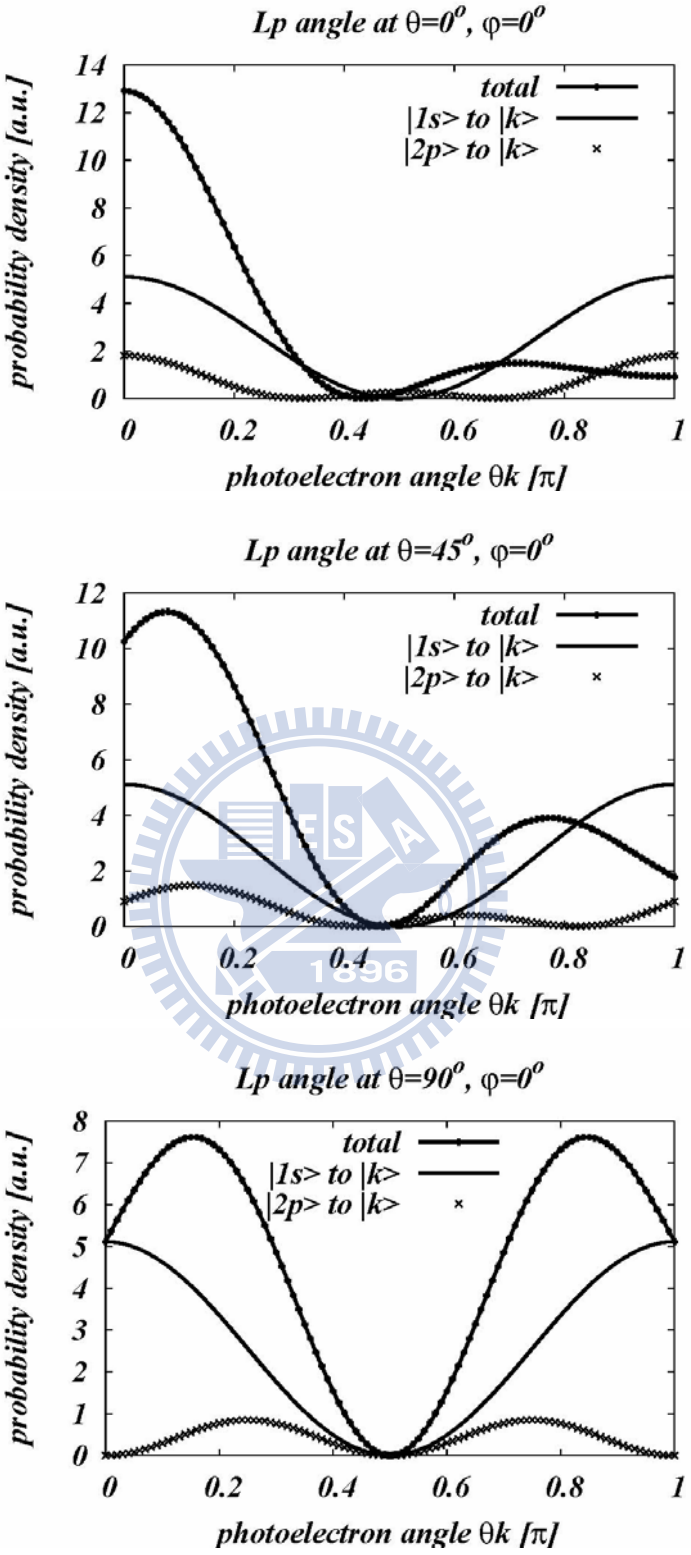

Figure. 5.3 The transition probability density at x-z plane and $\varphi_k = 0$ The line-points is the $|M_{if}|^2$, the line is the $|M_{k,1s}|^2$, and the points are the $|M_{k,2p}|^2 |M_{2p,1s}|^2$.

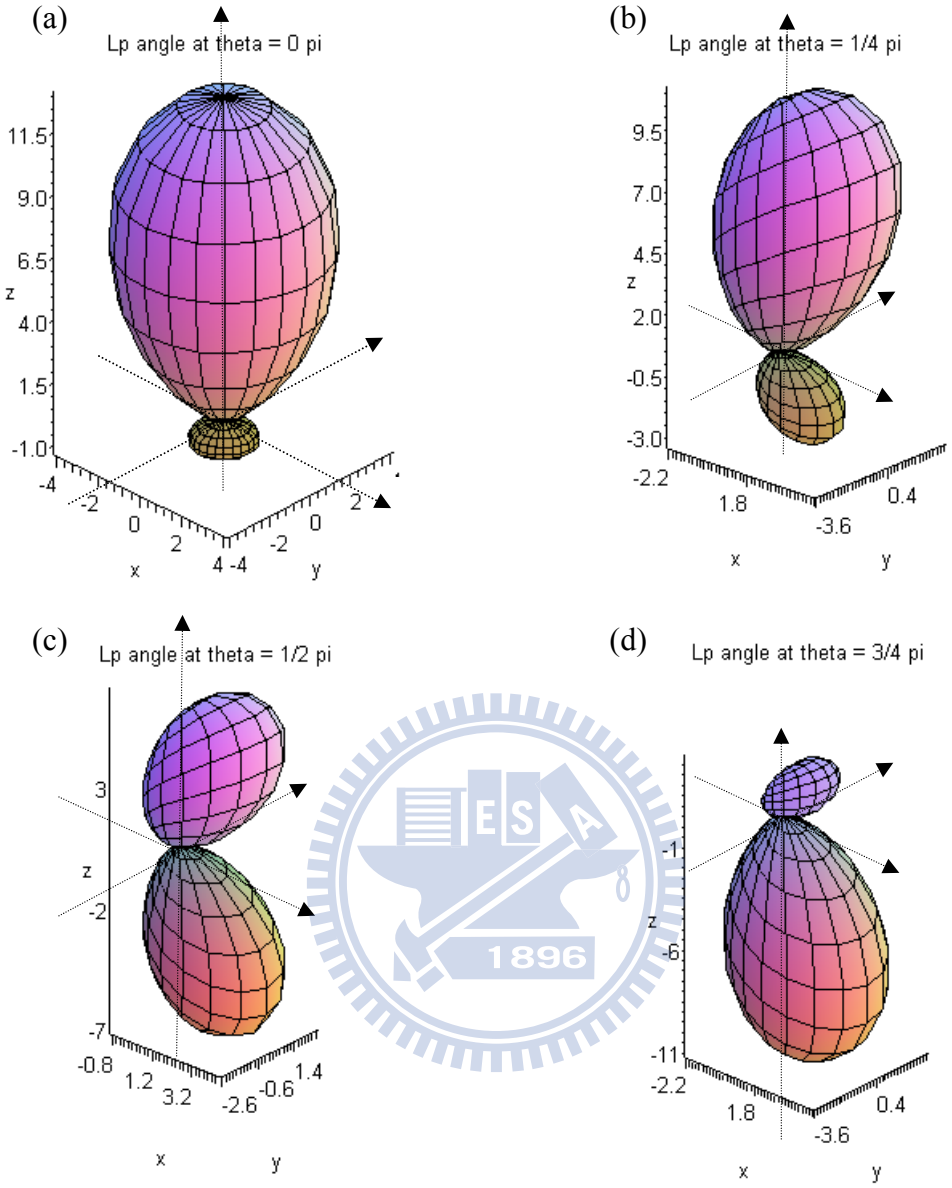

Figure. 5.4 The diagram on 3D space. Assigning a different direction on probe IR pulse to compute the transition probability density of Eqs.(5.3) dependence on photoelectron angle θ_k is about 0^o, 45^o and 90^o, at the time delay t_d = 7 fs and ε_k = 1.544 ev. (a) is aligned at θ_l=0^o, (b) 45^o , (c) 90^o , (d) 135^o

On the other hand, we focus on the terms of interference in Eqs. (5.1), and also find that only the 6th term of RHS is $\cos\theta_l$. Owing to this reason, only the 6th term will no be symmetric for θ_l changing to $\theta_l + \pi/2$. To figure out how terms of interference in Eqs. (5.3) are dependent on photoelectron angle θ_k, we show parts of interference in Eqs (5.3) dependence on the photoelectron angle θ_k in Fig. 5.5. From Fig. 5.5, because the value of 4th term is small over the θ_k, the 4th term has no contribution. Besides, the structure of 5th term is symmetric for the θ_l=45° to 150°, but the 6th term is not. When to change the photoelectron angle from θ_k to θ_k + π/2, the interference structure is mainly dependent on the 6th term which is from the spherical function $Y_{2,0}$ and $Y_{0,0}$ multiplying to $Y_{1,0}$ and all of them with same quantum number m. Furthermore, the interference depends on the 5th term when the φ_k changes to φ_k + π, because the coefficient A_1 includes $\cos(\varphi_k - \varphi_l)$, as showed in Eqs. (5.2). By parts of interference in Eqs. (5.1) to know what affect the interference constructively or destructively on left side (θ_k from 0 to $\pi/2$) and right side (θ_k from $\pi/2$ to π).

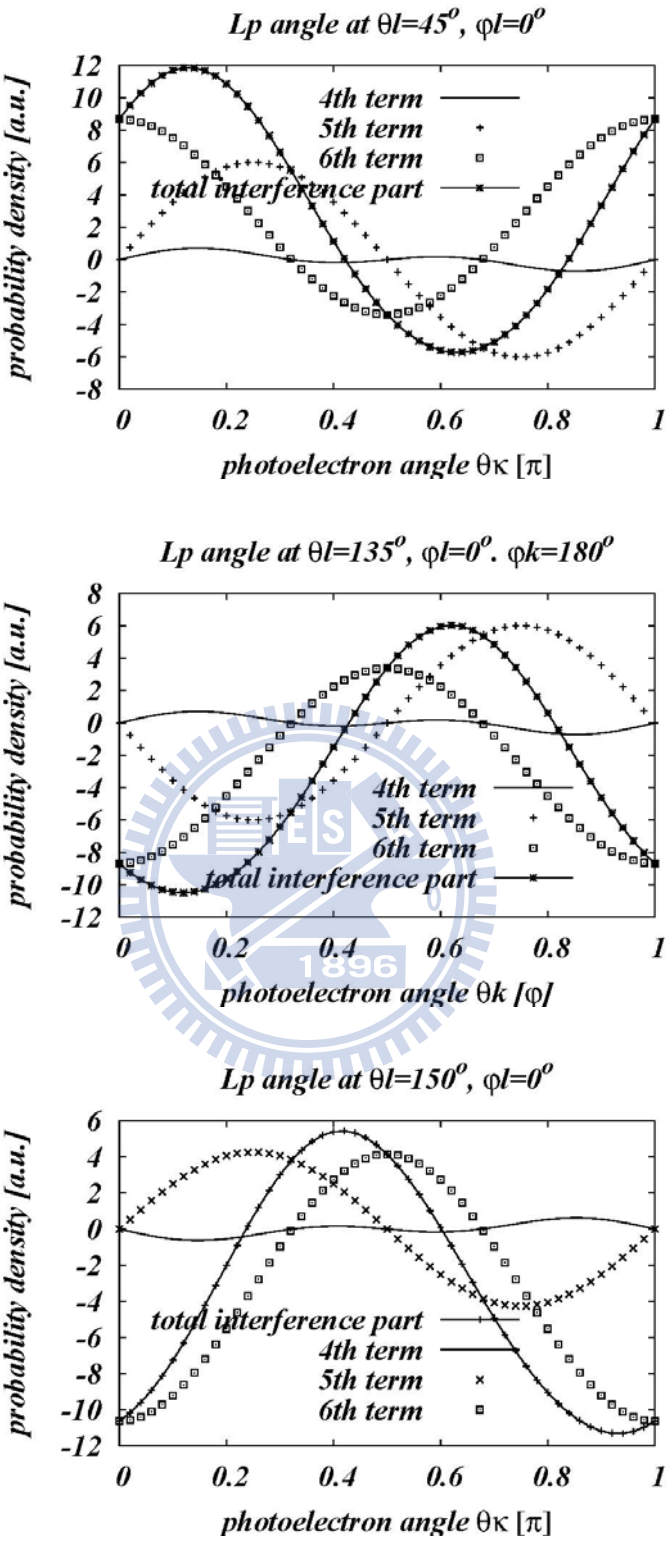

Figure. 5.5 The interference part of RHS in Eqs. (5.3). Only the spherical harmonic function with same quantum number m, the 6th term of RHS in Eqs. (5.3), multiplying with each other is dependent on the direction of IR laser pulse's polar angle, and the 5th term is dependent on the azimuth angle of photoelectron.

The coefficients of cosinusoidal and sinusoidal function are different in Eqs. (5.1) on different time delay t_d, and will contribute different interference. Accordingly, to change time delay can control the localization of emitting electron for particular energy. In Fig. 5.7, when assigning the probe IR laser pulse's direction at $\theta_l = 45^o$ and $\varphi_l = 0^o$, the transition probability density for photoelectron at $\theta_k = 45^o$ is smaller then $\theta_k = 135^o$ at time delay t_d = 5.76 fs, but at time delay t_d = 6.18 fs is larger then $\theta_k = 135^o$. Define the asymmetry parameter $A(\varepsilon_k)$ as the difference signal between momentum distribution at the θ_k being parallel and antiparallel to the probe IR laser pulse with a particular photoelectron energy ε_k.

$$A(\varepsilon_k) = \frac{p_{up} - p_{down}}{p_{up} + p_{down}} = \frac{|M_{if}(\theta_k, \varphi_k, \varepsilon_k)|^2 - |M_{if}(\pi - \theta_k, \pi + \varphi_k, \varepsilon_k)|^2}{|M_{if}(\theta_k, \varphi_k, \varepsilon_k)|^2 + |M_{if}(\pi - \theta_k, \pi + \varphi_k, \varepsilon_k)|^2} \tag{5.4}$$

where up p_{up} and p_{down} are

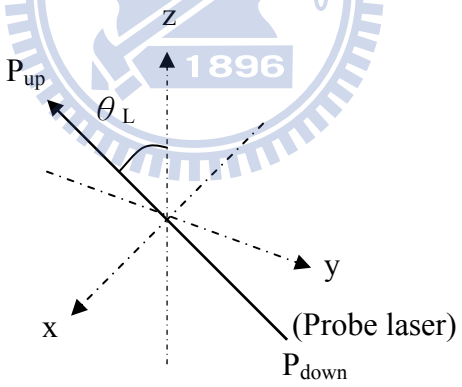

Figure. 5.6 The diagram for the asymmetry parameter

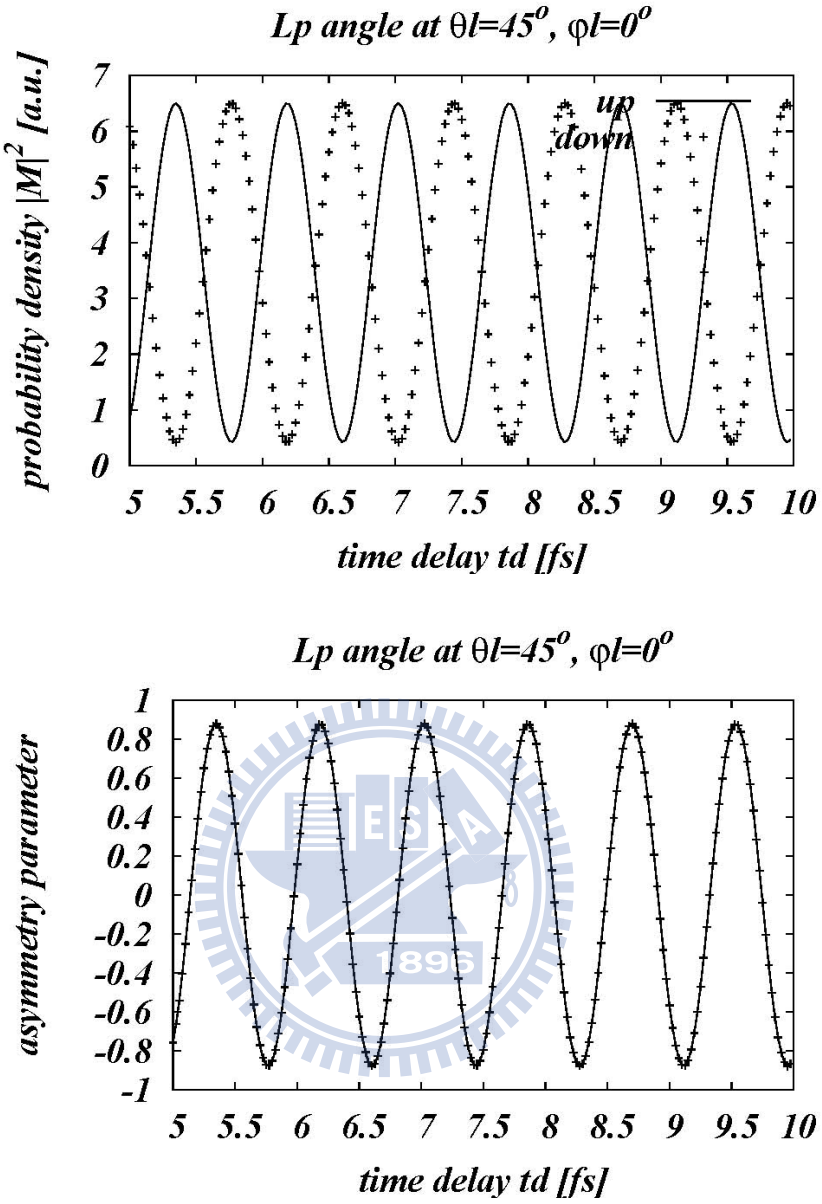

Figure. 5.7 The figure for transition probability density $|M_{if}|^2$ dependence on time delay t_d and asymmetry parameter. In upper figure, up is photoelectron angle at $\theta_k = 45^o$, $\varphi_k = 0^o$ and down is $\theta_k = 135^o$, $\varphi_k = 180^o$ with photoelectron energy ε_k =1.544 ev

As the paragraphs above, the phase can change the interference in Eqs. (3.8), furthermore to change the localization of electron. We can also change the CEP of IR laser pulse to change the interference.

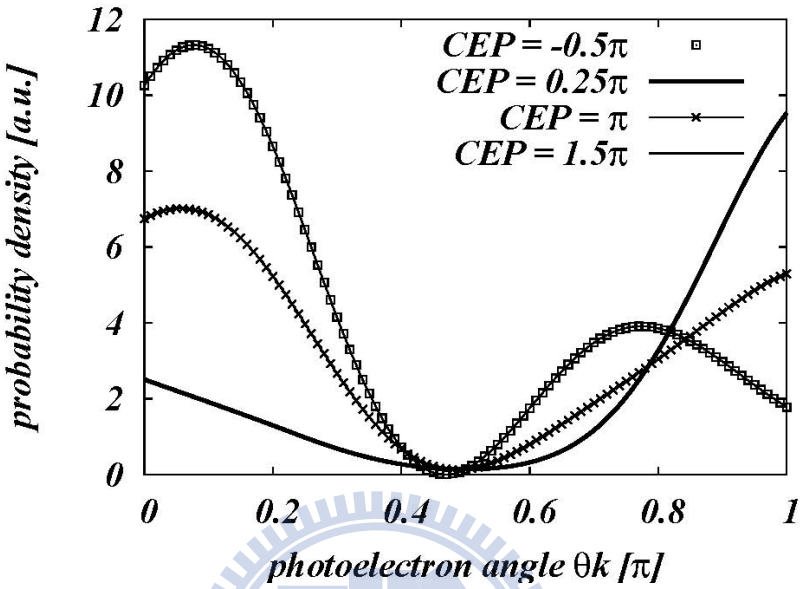

Figure. 5.8 The total probability density $|M_{if}|^2$ depdents on θ_k for different CEP. The ε_k = 1.544 ev, the t_d = 7fs and the IR laser pulse aligned to θ_l=0.25π.

From Fig. 5.8 the interference effect is changed by tuning the CEP of IR laser pulse. In Fig. (5.8), the probability density at CEP = -0.5π is the same as CEP = 1.5π = -0.5π + 2π, and there is the maximum value of total probability density over photoelectron angle θ_k when the CEP = 0.25π and the θ_k=π. This is because that the photon is mainly located at θ_k=π when the photoelectron energy is particular ε_k=1.544 ev and the CEP of IR lase pulse is equal 0.25π.

Some applications for alligning a special probe's IR laser pulse's direction is to reconstruct the transition probability density for the experimental observation. For $\theta_l = 90^o$,

$\varphi_l = 0^o$ and $\varphi_k = 90^o$, the probability density becomes

$$|M_{if}(\theta_l, \varphi_l)|^2 = B^2 \tag{5.5}$$

For $\theta_l = 0^o$, $\varphi_l = 0^o$ and $\varphi_k = 90^o$, the probability density becomes

$$|M_{if}(\theta_l, \varphi_l)|^2 = A_2^{\,2} + B^2 + 2A_2 B\cos(\varphi_b - \alpha_2) \tag{5.6}$$

For $\theta_l = 180^o$, $\varphi_l = 0^o$ and $\varphi_k = 90^o$, the probability density becomes

$$|M_{if}(\theta_l, \varphi_l)|^2 = A_2^{\,2} + B^2 - 2A_2 B\cos(\varphi_b - \alpha_2) \tag{5.7}$$

For $\theta_l = 90^o$, $\varphi_l = 0^o$ and φ_k = fix to an angle we want, the probability density becomes

$$|M_{if}(\theta_l, \varphi_l)|^2 = A_1^{\,2} + B^2 + 2A_1 B\cos(\varphi_b - \alpha_1) \tag{5.8}$$

For $\theta_l = 45^o$, $\varphi_l = 0^o$ and φ_k = fix to an angle as the same as Eqs. (5.7), the probability density becomes

$$\begin{aligned} |M_{if}(\theta_l, \varphi_l)|^2 = {} & \frac{A_1^{\,2}}{2} + \frac{A_2^{\,2}}{2} + B^2 + A_1 A_2\cos(\alpha_2 - \alpha_1) \\ & + \frac{2}{\sqrt{2}} A_1 B\cos(\varphi_b - \alpha_1) \\ & + \frac{2}{\sqrt{2}} A_2 B\cos(\varphi_b - \alpha_2) \end{aligned} \tag{5.9}$$

For $\theta_l = 135^o$, $\varphi_l = 0^o$ and φ_k = fix to an angle as the same as Eqs. (5.7), the probability density becomes

$$\begin{aligned} |M_{if}(\theta_l, \varphi_l)|^2 = {} & \frac{A_1^{\,2}}{2} + \frac{A_2^{\,2}}{2} + B^2 - A_1 A_2\cos(\alpha_2 - \alpha_1) \\ & + \frac{2}{\sqrt{2}} A_1 B\cos(\varphi_b - \alpha_1) \\ & - \frac{2}{\sqrt{2}} A_2 B\cos(\varphi_b - \alpha_2) \end{aligned} \tag{5.10}$$

Do not consider the change of Volkov phase in Eqs (5.5) to (5.10), because $\vec{\alpha} \cdot \vec{k}$ is too small to neglect in Eqs.(3.8), and use linear combination of the angle-resolved transition probability density from Eqs.(5.5) to (5.10) to reconstruct the information of $|M_{if}(\theta_l, \varphi_l)|^2$. In Fig. 5.9, when probe IR pulse is aligned to $\theta_l = 45^o$ and 135^o, the reconstruction well fits in with the

observation. Besides, we use reconstructed method not only can reconstruct the information for 1st and 2nd path, but also the parts of interference, as showed in Fig. 5.9.

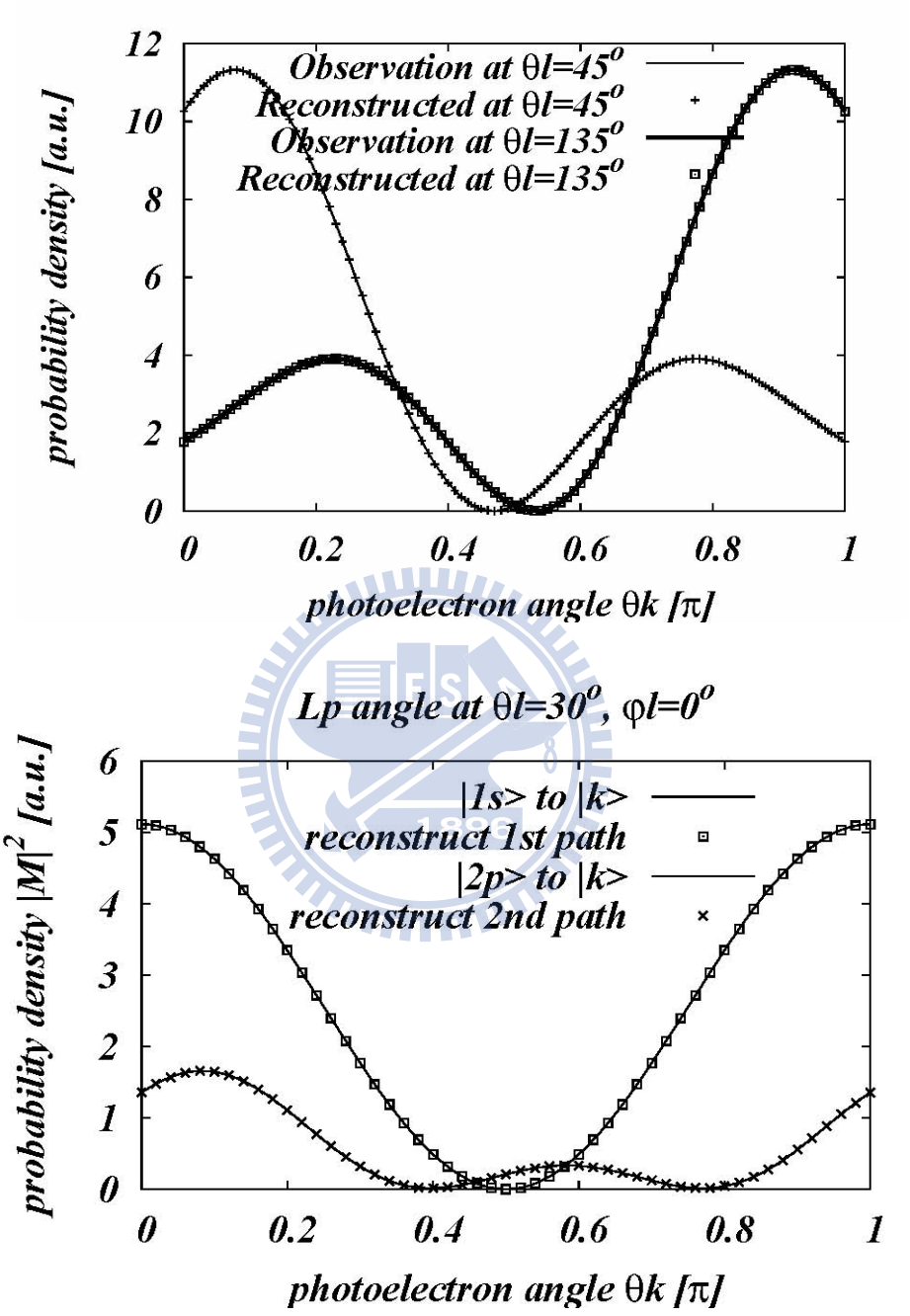

Figure. 5.9 To reconstruct the information from the experiment observation. The ε_k = 1.544 ev and the t_d = 7fs

Finally, we can investigate that the transition probability is dependent on the the direction of IR laser pulse. In Fig. 5.10, the minimum value of transition probability is about 24.65% when $\theta_l = 90^o$. This is because that after the pump APT pulse coming into the system, the electron cloud is polarized to the z-axis, and then get small ionization probability when the direction of IR pulse is perpendicular to the z-axis. On the contrary, aligning the direction of probe laser to parallel with the pump laser's direction will get more probability to ionize the electron. The probability formula is defined to

$$P = \int d\varepsilon_k \int | M_{i\to f} |^2 \, d\Omega_k \tag{5.11}$$

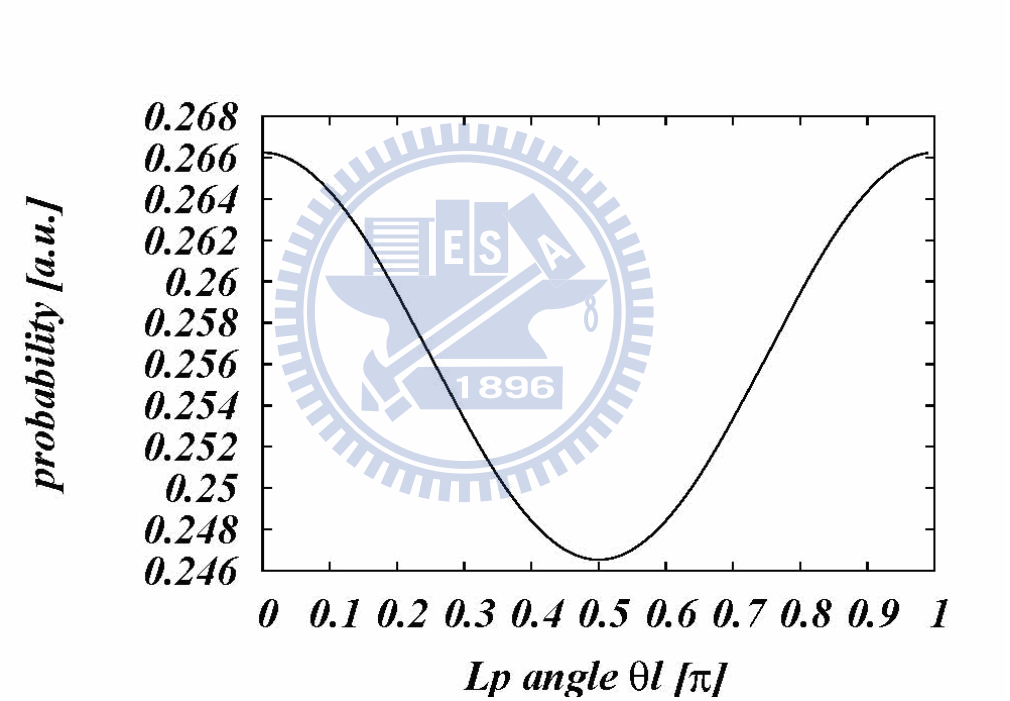

Figure. 5.10 The probability of ionization depends on the direction of IR laser pulse. There is a maximum value, when the direction of probe IR laser is aligned to parallel to the pump APT pulse, and oppositely there is a minimum value when the direction is aligned to perpendicular to the pump APT pulse.

5.2 Elliptical polarization

It is more interesting on using elliptical polarization on the probe IR pulse. The probe IR pulse is changed to the form of elliptical polarization as

$$H'_{probe} = E_x\hat{x} + E_z\hat{z} = E_0 \cdot \exp[-2\ln 2(t/\tau_L)^2] \times \left[\frac{1}{\sqrt{1+\alpha^2}}\cos(\omega t + \varphi_L)\cdot\hat{z} + \frac{\alpha}{\sqrt{1+\alpha^2}}\sin(\omega t + \varphi_L)\cdot\hat{x} \right] \quad (5.12)$$

where the α is the elliptical parameter and equals the ratio of the maximum amplitude E_x / E_z and the transition probability amplitude is

$$M_{if}(\theta_l,\varphi_l) = ia_1 e^{i\varphi_1}\{\, Y_{2,-1}(\Omega_k) + Y_{2,1}(\Omega_k)\,\}\frac{\alpha}{\sqrt{1+\alpha^2}} + \{\, a_2 e^{i\varphi_1} Y_{2,0}(\Omega_k) + a_3 e^{i\varphi_2} Y_{0,0}(\Omega_k)\,\}\frac{1}{\sqrt{1+\alpha^2}}{}_l + be^{i\varphi_b} Y_{1,0}(\Omega_k) \quad (5.13)$$

For clarity, rederive the Eqs. (5.12) as

$$M_{if}(\theta_l,\varphi_l) = iXe^{i\varphi_X}\frac{\alpha}{\sqrt{1+\alpha^2}} + Ze^{i\varphi_Z}\frac{\alpha}{\sqrt{1+\alpha^2}} + Be^{i\varphi_b} \quad (5.14)$$

where

$$\begin{aligned} X &= a_1\{\, Y_{2,-1}(\Omega_k) + Y_{2,1}(\Omega_k)\,\} \\ \varphi_X &= \varphi_1 \\ Ze^{i\varphi Z} &= \{\, a_2 e^{i\varphi_1} Y_{2,0}(\Omega_k) + a_3 e^{i\varphi_2} Y_{0,0}(\Omega_k)\,\} \\ B &= bY_{1,0}(\Omega_k) \end{aligned} \quad (5.15)$$

and the transition probability density is

$$|M_{if}(\theta_l,\varphi_l)|^2 = X^2\frac{\alpha^2}{1+\alpha^2} + Z^2\frac{1}{1+\alpha^2} + B^2 + 2XZ\sin(\varphi_Z-\varphi_X)\frac{\alpha}{1+\alpha^2} + 2XB\sin(\varphi_b-\varphi_X)\frac{\alpha}{\sqrt{1+\alpha^2}} + 2ZB\cos(\varphi_b-\varphi_Z)\frac{1}{\sqrt{1+\alpha^2}} \quad (5.16)$$

In Eqs. (5.16), the transition probability density is quite the same as linear polarization effect, if you let the $\frac{\alpha}{\sqrt{1+\alpha^2}} = \sin(\mu)$. In addition, the only difference between linear and elliptical polarization is the interference part, the fourth and fifth term of RHS in Eqs. (5.16). The phase which is dependent on time delay t_d and photoelectron energy ε_k in the fifth and the sixth term in Eqs (5.16) is the same as using linear polarization and equals $(\varepsilon_k - E_{2p}) \cdot t_d$, so the number of fringes in t_d from 5 to 15 fs is the same as linear polarization, as showed in Fig. 5.11.

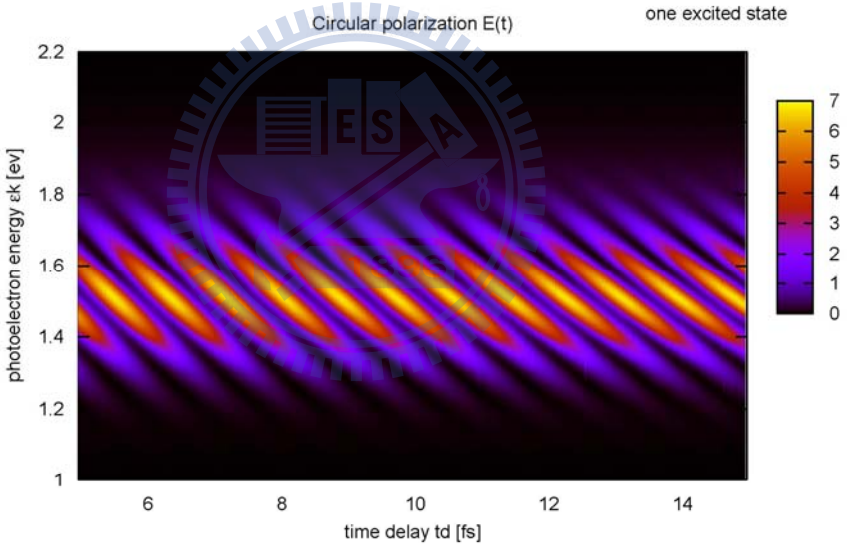

Figure. 5.11 To compare the Fig. (5.1), the number of fringe is the same as linear polarization in time delay t_d from 5 to 15 fs, but different to the structure of fringes.

Fig. 5.13 is the interference process contributed from the first and second path. The first and second path interfere constructively on the left side, but destructively on the righ side. In Fig. 5.13 and 5.14, which is showed that the photon cloud of probability density at ε_k=1.544

ev interfere with the first path and second path in 3D diagram. To compare the elliptical parater α = 1 and α = 2, the form for α = 2 in Fig. 5.15 is looked like sphericity then α = 1. This is because that when the elliptical parameter α =2 , the amplitude of electric field on x-axis direction ,$E_{x,}$ is twice of the amplitude on z-axis direction ,E_z, and the electron has higher probability to ionize to the x-axis direction, and then the form of probability density is looked like sphericity then α = 1.

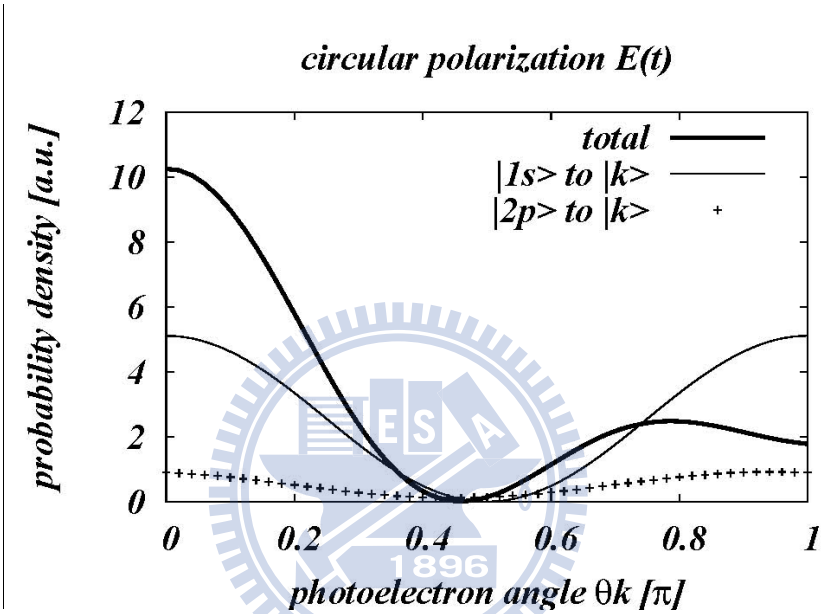

Figure. 5.12 The interference depends on photoelectron angle θ_k at ε_k=1.544 ev and the t_d = 7 fs. The thick line is total probability density, $|M_{i\to f}|^2$ the thin line is $|M_{k,1s}|^2$ and the points (+) is $|M_{k,2p}|^2|M_{2p,1s}|^2$.

For the same reason to figure out what are the main part contributing on the interference, we draw the the interference part in Eqs. (5.16). From Fig. 5.16, the first term of RHS in Eqs. (5.16) is no contribution to the interference and the mainly contribution to the interference is about the 6th term of RHS in Eqs. (5.16), the same as linear polarization case, interfering each other with the same quantum number m.

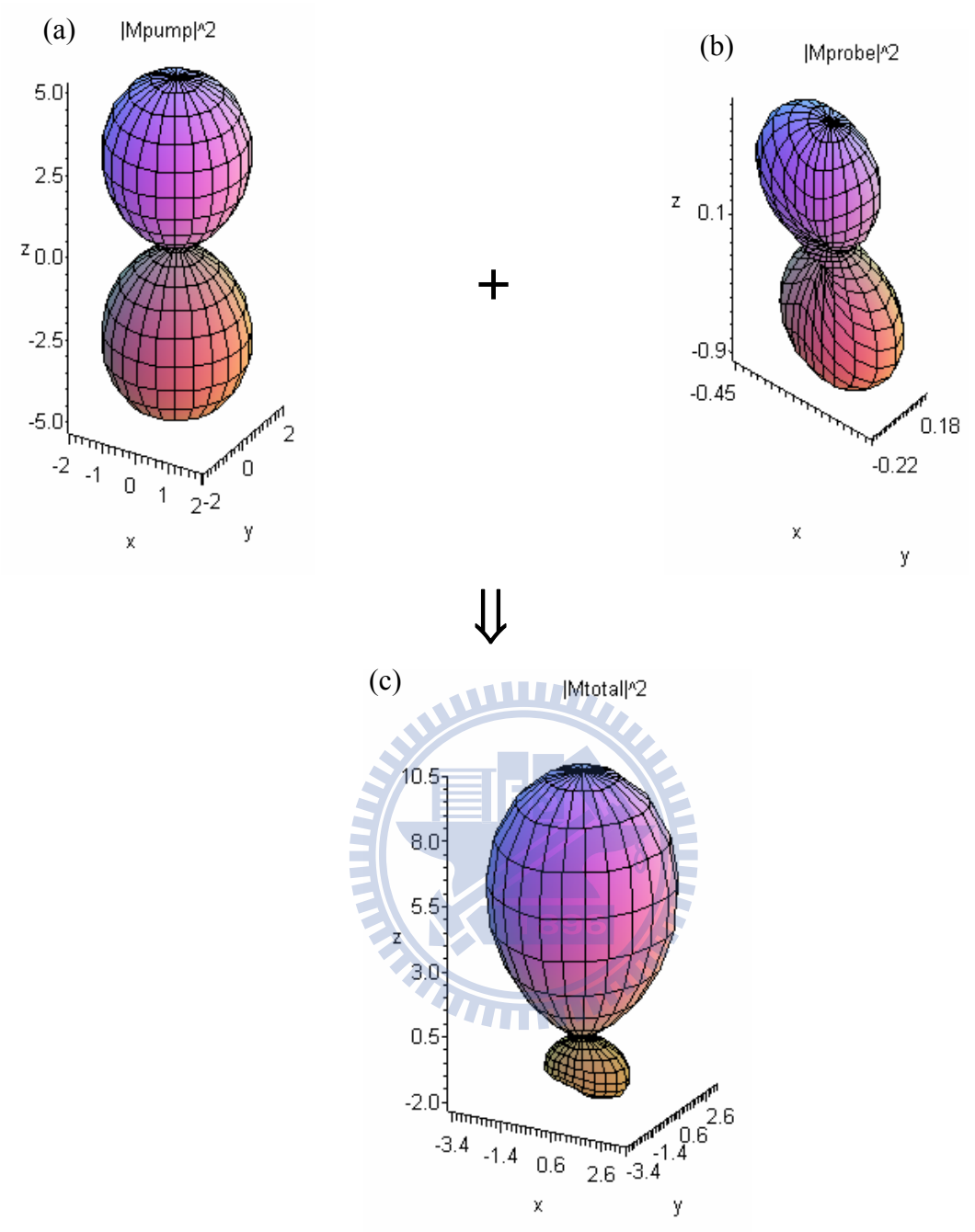

Figure. 5.13 The 3D digram is (a) first path, $|M_{k,1s}|^2$ by APT pulse, (b) second path, $|M_{k,2p}|^2|M_{2p,1s}|^2$ by circular polarization IR laser pulse (α=1) and (c) total path, $|M_{k,1s}+M_{k,2p}M_{2p,1s}|^2$ by the first and second path interfering with each other on the time delay t_d = 7 fs and ε_k = 1.544 ev.

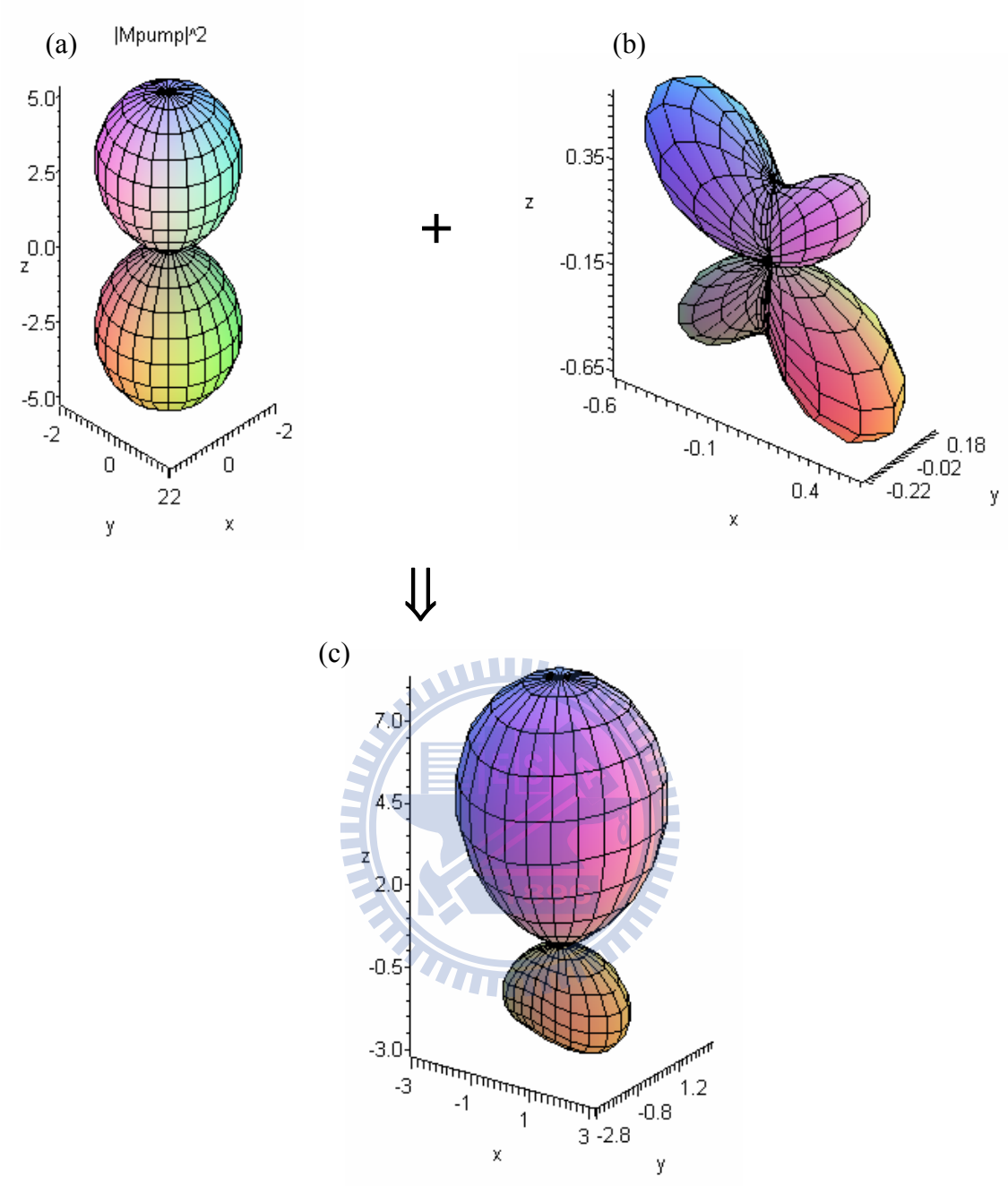

Figure. 5.14 The 3D digram is (a) first path, $|M_{k,1s}|^2$ by APT pulse, (b) second path, $|M_{k,2p}|^2|M_{2p,1s}|^2$ by elliptical polarization IR laser pulse (α=2) and (c) total path, $|M_{k,1s}+M_{k,2p}M_{2p,1s}|^2$ by the first and second path interfering with each other on the time delay t_d = 7 fs and ε_k = 1.544 ev.

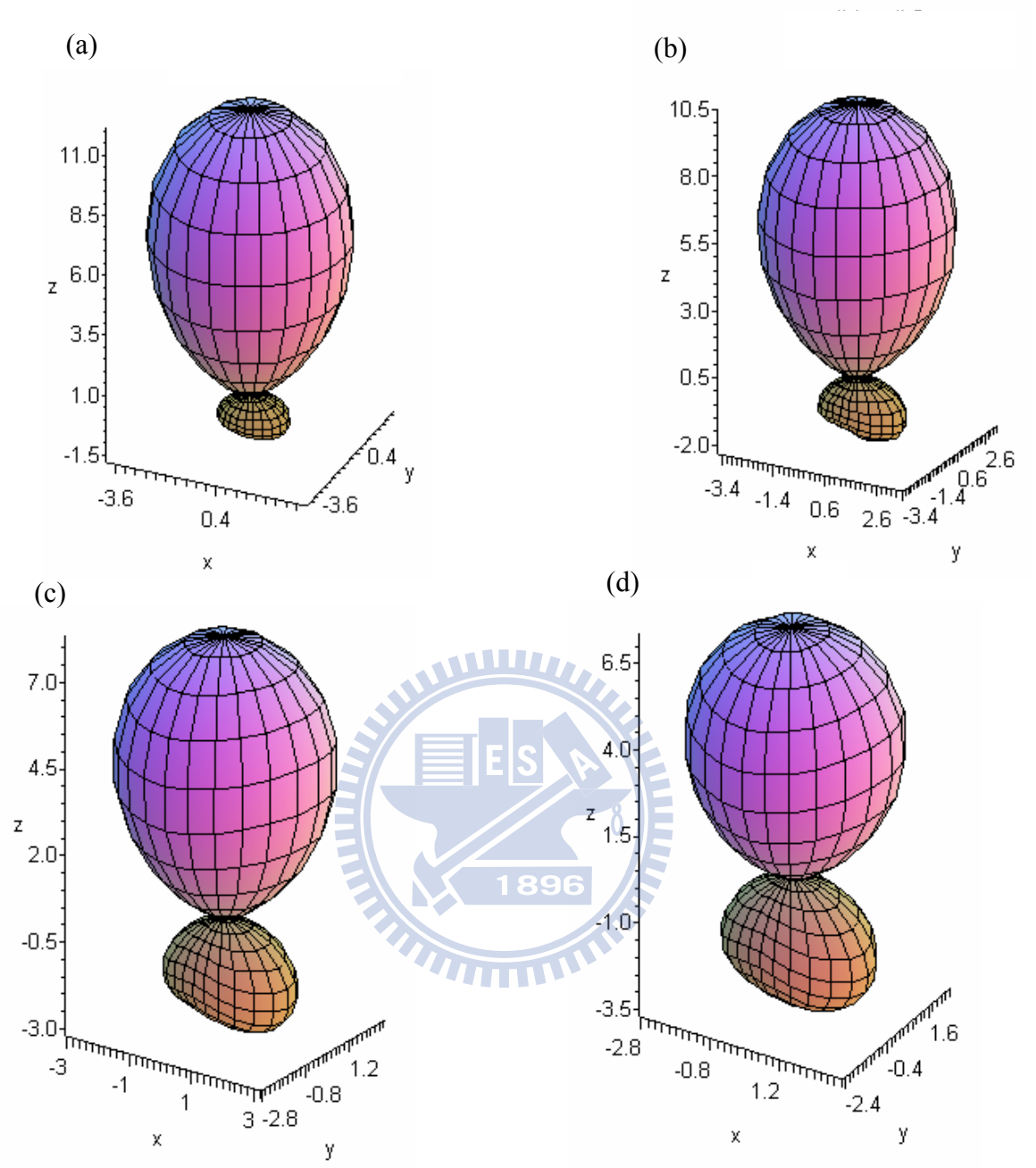

Figure. 5.15 The 3D digram for probability density $|M_{k,1s} + M_{k,2p}M_{2p,1s}|^2$ dependent on different elliptical parameter α, (a) α=0.5, (b) α=1, (c) α=2, (d) α=3. The structure of probability density which look like circular ball when elliptical parameter α is large. The parameter is time delay t_d = 7 fs and ε_k = 1.544 ev.

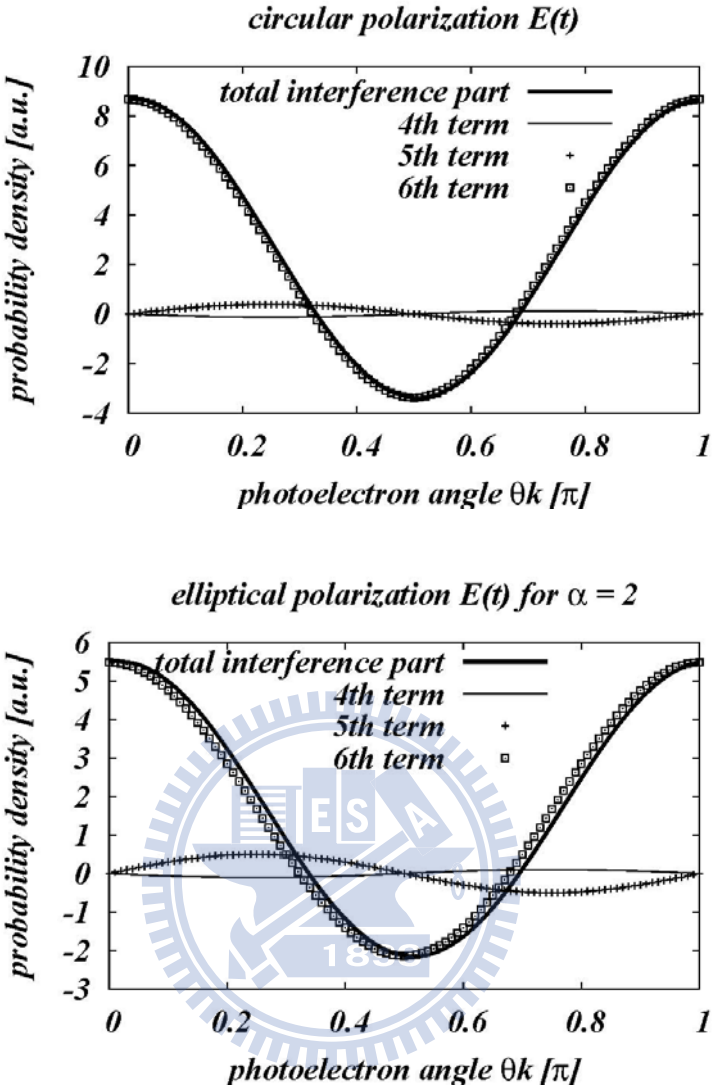

Figure. 5.16 The interference part of RHS in Eqs. (5.15). As the same as linear polarization case, the 6th term is the leading part for the interference.

The elliptical parameter α is the ratio of maximum amplitude for x and z direction of probe laser pulse, $\alpha = E_x / E_z$. As the same as using linear polarization on probe laser, the probability density when aligning the probe IR pulse to be perpendicular to pump APT pulse is smaller than to parallel with pump APT pulse. In Fig. 5.17, the probability density on left side has minimum value, but on right side is oppositely maximum value when α = 0.5. Therefore, try to calculate the probability of ionization depdent on elliptical parameter, as

showed in Fig. 5.18.

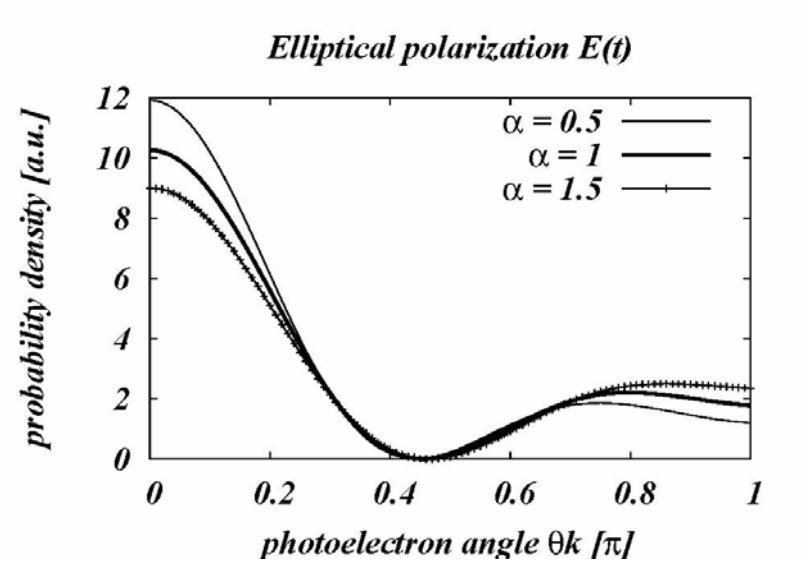

Figure. 5.17 The probability density $|M_{i\to f}|^2$ depdents on photoelectron angle θ_k. When the α grow up, the form will be like circule (see Fig. 5.15), so the value of probability density at θ_k =0° will gradually be near to 180°.

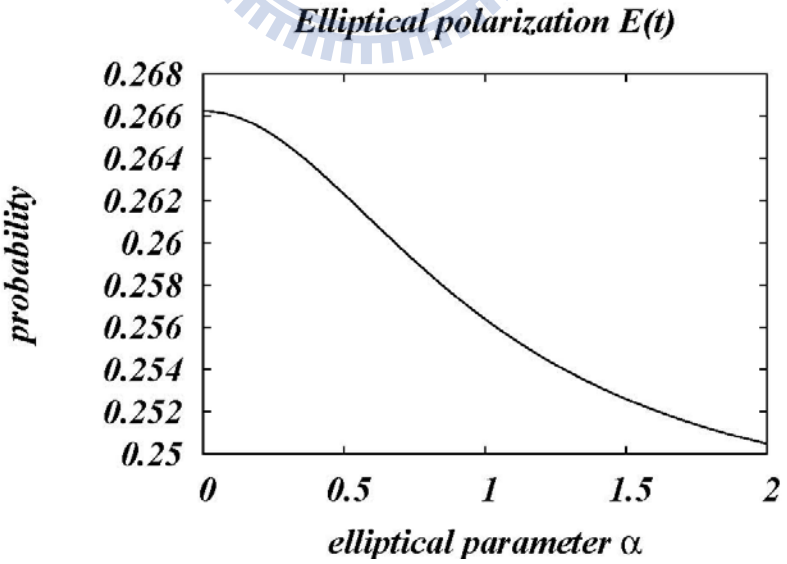

Figure. 5.18 The total probability of ionization which is dependent on elliptical parameter is sliding down when α grows up gradually.

Finally, we show the transition probability density which is dependent on the photoelectron's momentum in x-axis and z-axis direction to see the localization of photon when aligning different polarized direction on probe IR laser pulse. In Fig. 5.19, when aligning the direction of probe laser to parallel with the z-axis, the probability density mainly distributes around to the top of the z-axis; when to be perpendicular to the z-axis, the region of probability density is larger then to parallel with z-axis. Besides, In Fig. 5.19.a, there are higher probability density on z direction then Fig. 5.19.c. This is because that the electron is driven to the x direction by the probe laser when $\theta_l = 90^o$, and have weaker signal on the z-axis then when $\theta_l = 0^o$. When aligning the direction of probe laser not to parallel and not be perpendicular to the z-axis, the most distribution of probability density is not on the z-axis, but on the angle between pump laser's and probe laser's polarized direction.

From Fig. 5.19 and 5.20, which are showed that the effect of linear compare to elliptical polarization to see the localization of photoelectron. In Fig. 5.20, the most probability density is around to the top of the z-axis, as the same as $\theta_l = 0$, when the polarized direction of probe laser is circular polarization. To use circular polarization on probe laser, the direction of probe laser changes with time's evolution, so the direction for electron tunneling out the coulomb potential is around the space. That's why the probability density for probe laser on circular polarization is average, and the red area not on the fringe in Fig. 5.20 is smaller then Fig. 5.19. On the other hand, when the elliptical parameter α=5 is larger then α=1, the region of red color is larger then α=1. This it because that the electric pulse's amplitude on x direction is quintuple amplitude on z direction, and electron have more chance to tunnel to the x direction, as showed in Fig. 5.20.

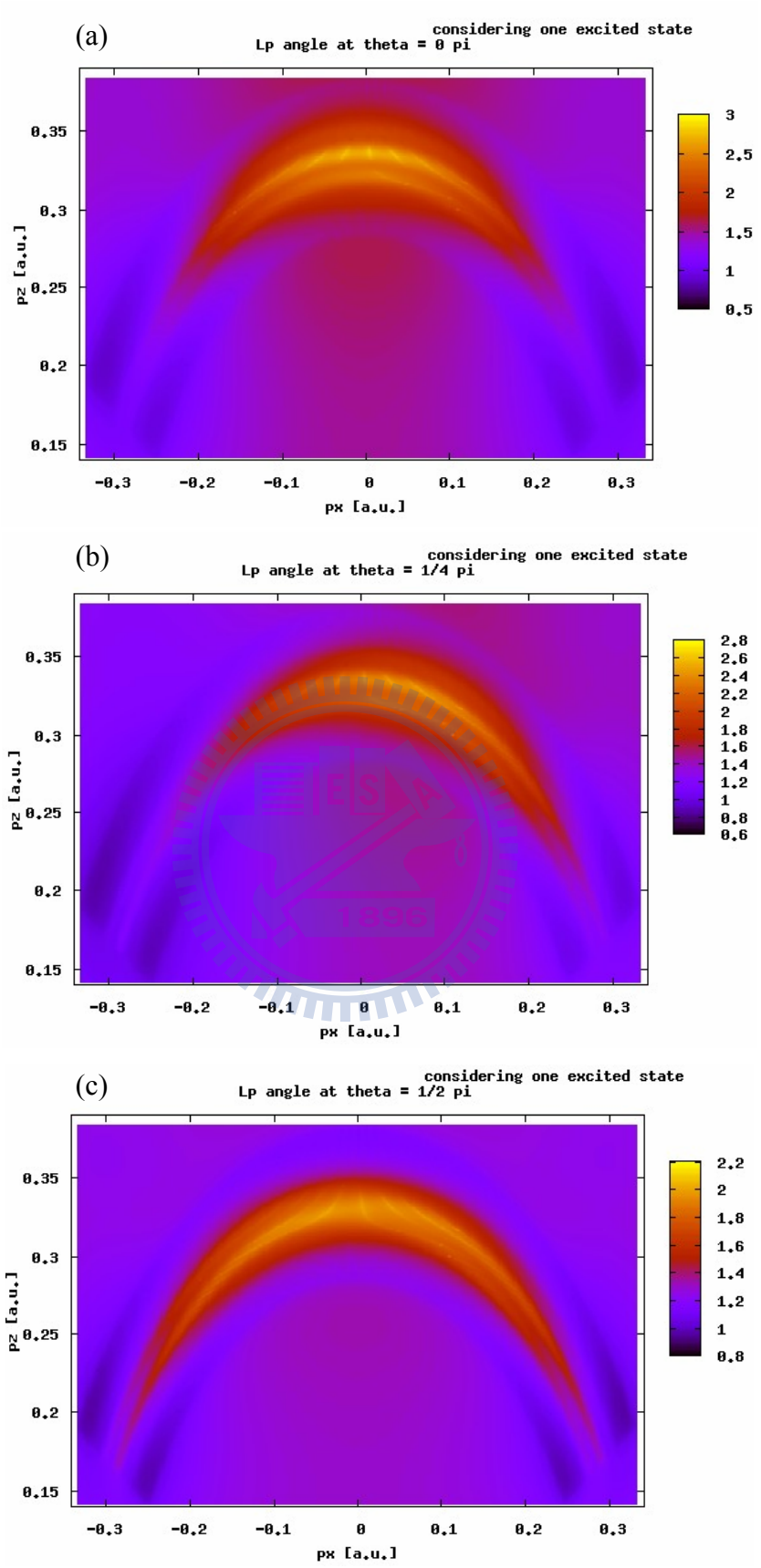

Figure. 5.19 The transition probability density depends on the x and z direction momentum of photoelectron, p_x and p_z. (a) θ_l = 0^o, (b) θ_l = 45^o, (c) θ_l = 90^o.

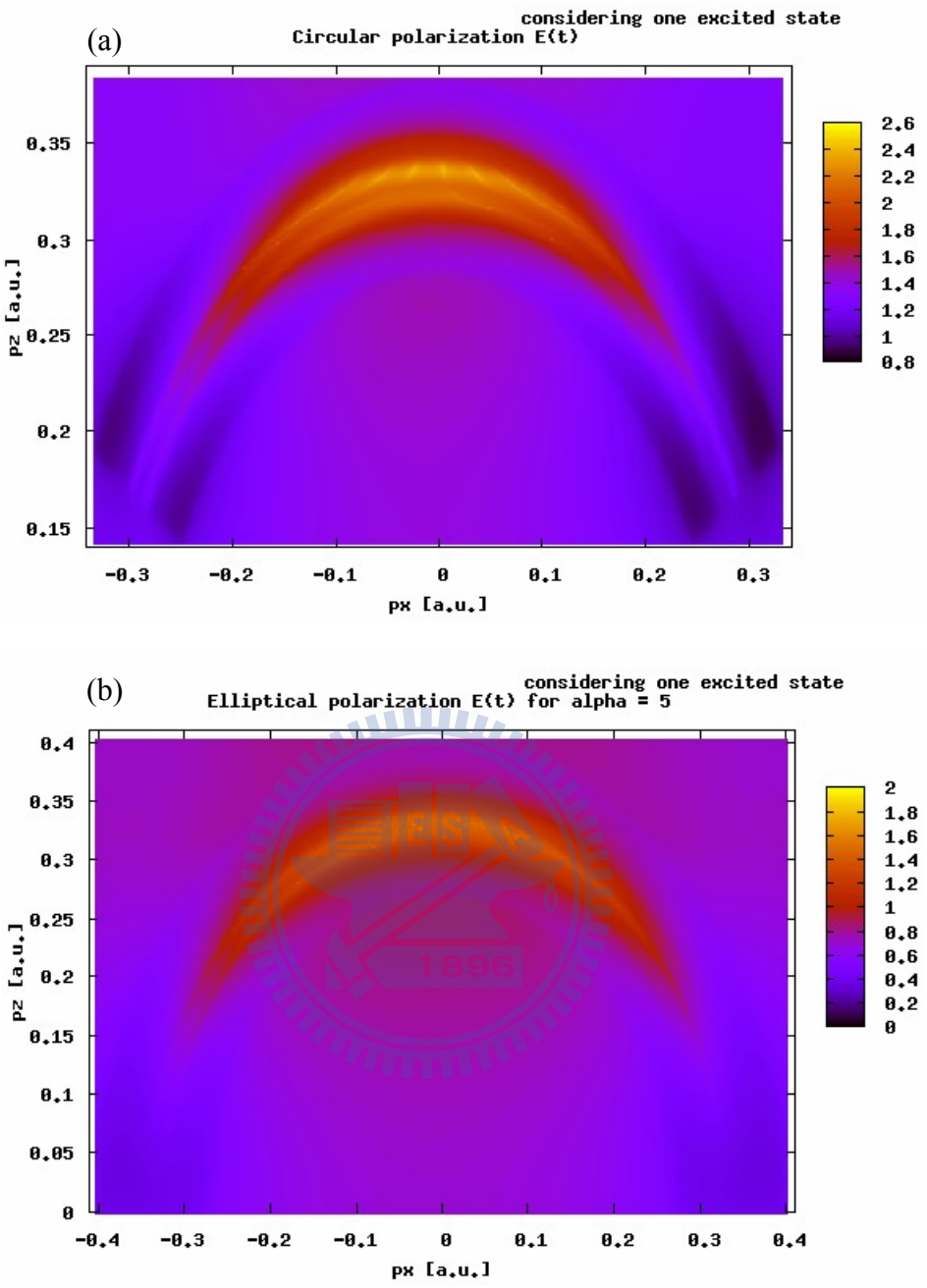

Figure. 5.20 The transition probability density depends on the x and z direction momentum of photoelectron, p_x and p_z . (a) Elliptical polarization for α=1, (b) α=5.

Chapter 6

Conclusions

In this thesis, we investigated that interference fringes for considering one and two excited state in pump-probe model were hyperbola structure as the same as the [1], but the frequency of the fringes appealing when time delay t_d from 5 fs to 15 fs was not the same between considering one and two excited state. Secondly, the localization of photon can be controlled by aligning the IR laser pulse at different direction and by controlling the phase with tuning the time delay t_d and CEP of IR laser pulse. In addition, the total probability of ionization was maximum value when IR laser pulse aligned to parallel to the APT pulse, but miminum for aligning probe laser to be perpendicular to the pump laser. Besides, we used reconstructed method to simulate signal data for any direction very well by using the linear combination of the detected experimental data.

On the other hand, for using the elliptical polarization, the partial probability density $|M_{k,2p}|^2|M_{2p,1s}|^2$ by IR laser pulse was roughly average effect for every direction, so the maximum of total transition probability density was always at photoelectron angle θ_k=0 or π, not the same on linear polarization. This is because of the interference part almost contributed by only term, the 6th of RHS in Eqs. (5.16). Furthermore, when the elliptical parameter α grown up ,then the form of the probability density in 3D diagram at particular photoelectron energy will look like circule on x-z plane. The total ionization probability was sliding down when the elliptical parameter is grown up.

Reference

[1] N. N. Choi, T. F. Jiang, Toru Morishita, M. H. Lee, and C. D. Lin, “Theory of probing attosecond electron wave packets via two-path interference”, PRA (accepted, 2010)

[2] P. Ranitovic, etc. “IR-assisted ionization of helium by attosecond extreme ultraviolet radiation” New Journal of Physics 12, 013008, 2010

[3] Marlan O. Scully and M. Suhail Zubairy, “Quantum Optics”, 1997

[4] N. Michel, “Precise Coulomb wave functions for a wide range of complex l, η and z^*” ”, CPC ,176, 232 – 249, 2007

[5] J. Mauritsson, T. Remetter, M. Swoboda, K. Klunder, A. L’Huillier, K. J. Schafer, “Attosecond electron spectroscopy using a novel interferometric pump-probe technique” (Submitted on 7 Jan2010, last revised 4 Jun 2010)

Appendix A

In Eqs. (4.4) the coefficient define to

$$A_{3p} = \frac{E_0}{2}\exp\left\{ \frac{[\omega_{probe} - (\varepsilon_k - E_{3p})]^2}{8\ln 2/\tau_L^{\,2}} \right\}\sqrt{\frac{\pi\tau_L^{\,2}}{2\ln 2}} \mid M_{3p,1s} \mid \sqrt{\frac{4\pi}{15}}\cdot\int r^2 F_2^{\,*} R_{31} dr \cdot Y^*_{1,-1}(\Omega_l)$$

$$B_{3p} = \frac{E_0}{2}\exp\left\{ \frac{[\omega_{probe} - (\varepsilon_k - E_{3p})]^2}{8\ln 2/\tau_L^{\,2}} \right\}\sqrt{\frac{\pi\tau_L^{\,2}}{2\ln 2}} \mid M_{3p,1s} \mid \sqrt{\frac{4\pi}{15}}\cdot\int r^2 F_2^{\,*} R_{31} dr \cdot Y^*_{1,1}(\Omega_l)$$

$$C_{3p} = \frac{E_0}{2}\exp\left\{ \frac{[\omega_{probe} - (\varepsilon_k - E_{3p})]^2}{8\ln 2/\tau_L^{\,2}} \right\}\sqrt{\frac{\pi\tau_L^{\,2}}{2\ln 2}} \mid M_{3p,1s} \mid \frac{3}{4}\sqrt{\frac{\pi}{5}}\cdot\int r^2 F_2^{\,*} R_{31} dr$$

$$D_{3p} = \frac{E_0}{2}\exp\left\{ \frac{[\omega_{probe} - (\varepsilon_k - E_{3p})]^2}{8\ln 2/\tau_L^{\,2}} \right\}\sqrt{\frac{\pi\tau_L^{\,2}}{2\ln 2}} \mid M_{3p,1s} \mid \frac{2}{3}\sqrt{\pi}\cdot\int r^2 F_0^{\,*} R_{31} dr$$

$$A_{4p} = \frac{E_0}{2}\exp\left\{ \frac{[\omega_{probe} - (\varepsilon_k - E_{4p})]^2}{8\ln 2/\tau_L^{\,2}} \right\}\sqrt{\frac{\pi\tau_L^{\,2}}{2\ln 2}} \mid M_{4p,1s} \mid \sqrt{\frac{4\pi}{15}}\cdot\int r^2 F_2^{\,*} R_{31} dr \cdot Y^*_{1,-1}(\Omega_l)$$

$$B_{4p} = \frac{E_0}{2}\exp\left\{ \frac{[\omega_{probe} - (\varepsilon_k - E_{4p})]^2}{8\ln 2/\tau_L^{\,2}} \right\}\sqrt{\frac{\pi\tau_L^{\,2}}{2\ln 2}} \mid M_{4p,1s} \mid \sqrt{\frac{4\pi}{15}}\cdot\int r^2 F_2^{\,*} R_{31} dr \cdot Y^*_{1,1}(\Omega_l)$$

$$C_{4p} = \frac{E_0}{2}\exp\left\{ \frac{[\omega_{probe} - (\varepsilon_k - E_{4p})]^2}{8\ln 2/\tau_L^{\,2}} \right\}\sqrt{\frac{\pi\tau_L^{\,2}}{2\ln 2}} \mid M_{4p,1s} \mid \frac{3}{4}\sqrt{\frac{\pi}{5}}\cdot\int r^2 F_2^{\,*} R_{31} dr$$

$$D_{4p} = \frac{E_0}{2}\exp\left\{ \frac{[\omega_{probe} - (\varepsilon_k - E_{4p})]^2}{8\ln 2/\tau_L^{\,2}} \right\}\sqrt{\frac{\pi\tau_L^{\,2}}{2\ln 2}} \mid M_{4p,1s} \mid \frac{2}{3}\sqrt{\pi}\cdot\int r^2 F_0^{\,*} R_{31} dr$$

$$E_{1s} = -\frac{E_m}{2}\exp\left\{ \frac{[\omega_{pump} - (\varepsilon_k - E_{1s})]^2}{8\ln 2/\tau_x^{\,2}} \right\}\sqrt{\frac{\pi\tau_x^{\,2}}{2\ln 2}}\cdot\int r^2 F_1^{\,*} R_{10} dr$$

$$\delta_1 = \phi_{3p} - t_d E_{3p} + \sigma_2 + (\varepsilon_k - E_{3p})\frac{\tau_L}{2} - \varphi_L - \frac{\pi}{2}$$

$$\delta_2 = \phi_{3p} - t_d E_{3p} + \sigma_0 + (\varepsilon_k - E_{3p})\frac{\tau_L}{2} - \varphi_L - \frac{\pi}{2}$$

$$\eta_1 = \phi_{4p} - t_d E_{4p} + \sigma_2 + (\varepsilon_k - E_{4p})\frac{\tau_L}{2} - \varphi_L - \frac{\pi}{2}$$

$$\eta_2 = \phi_{4p} - t_d E_{4p} + \sigma_0 + (\varepsilon_k - E_{4p})\frac{\tau_L}{2} - \varphi_L - \frac{\pi}{2}$$

$$\beta_{1s} = (\varepsilon_k - E_{1s})\frac{\tau_X}{2} - \phi_X + \sigma_1 - (t_d\varepsilon_k + \tau_L\varepsilon_k + \vec{\alpha}\cdot\vec{k} + \beta)$$